博士論文

Investigation of Corrosion Behavior of Ni-free Stainless Steel for Use of Bipolar Plate in Polymer Electrolyte Fuel Cell

（固体高分子形燃料電池用金属セパレータとしてのNiフリーステンレス鋼の耐食性評価）

長岡技術科学大学大学院工学研究科
エネルギー•環境工学専攻
于　洋

Acknowledgements

Firstly, I would like to express my sincere appreciation to my supervisor Prof. Umeda for the continuous support and guidance of my Ph.D study and research, for his patience, motivation, enthusiasm, and immense knowledge, without which this work would not have been possible.

I am very truly grateful to my co-supervisor Assoc. Prof. Shironita, her guidance helped me in all the time of research and writing of this thesis. Her assistance has helped me to overcome difficulty in my life and given me encourage. Also to Prof. Soma, Prof. Matsubara, Prof. Imakubo and Prof. Tagaya as my examiners who gave me insightful comments through the defense of this thesis.

Besides my supervisors, I am very thankful to the assistance of the other staffs from my laboratory and Nagaoka University of Technology for their help whenever I need.

I would like to thank all the members of the laboratory for the stimulating discussions, all the fun we have had, and the help they have given me in my three years life here. Also I thank my friends in Nagaoka University of Technology.

Last but not the least, I would like to thank my family, especially my parents and my sister for supporting me spiritually throughout my life.

于 洋

Contents

Chapter 1 Introduction

1.1 Fuel cells

1.1.1 A brief introduction to fuel cells

Fuel cells are electrochemical devices that use the chemical properties of a gaseous fuel (hydrogen) and an oxidant gas (typically oxygen from the air) to directly create electrochemical current, the electrical power [1,2]. Fuel cells work technically similar to batteries in its basic principles, but unlike batteries. The difference from a battery is that as long as the stored externally fuel and oxidant are supplied, the fuel cell will continue producing energy and does not require recharging or run down. However, the internal energy storage limits the capacity of a battery [3]. Compared to other conventional thermo-mechanical systems, fuel cells can offer more electricity from the same amount of fuel, giving much higher conversion efficiencies [4].

Most fuel cell systems is considered by a number of components [5]:

- Unite cells.

  The unite cells are the core of a fuel cell, where the electrochemical reactions happen. The basic structure of a fuel cell comprises an anode (negative electrode) and a cathode (positive electrode) on either side in contact with an electrolyte layer. A schematic image of a unite cell is shown in Figure 1-1 [6]. Fuel is supplied to the anode and an oxidant gas is supplied to the cathode. The electric current is generated from the electrochemical reactions taken place at the electrodes through the electrolyte. The chemical reactions in the

anode and cathode are [7]

$$\text{Anode reaction:} \quad H_2 \rightarrow 2H^+ + 2e^- \tag{1-1}$$

$$\text{Cathode reaction:} \quad O_2 + 4H^+ + 4e^- \rightarrow 2H_2O \tag{1-2}$$

The overall reaction for hydrogen/oxygen (air) fuel cells is given as [8]

$$2H_2 + O_2 \rightarrow 2H_2O \tag{1-3}$$

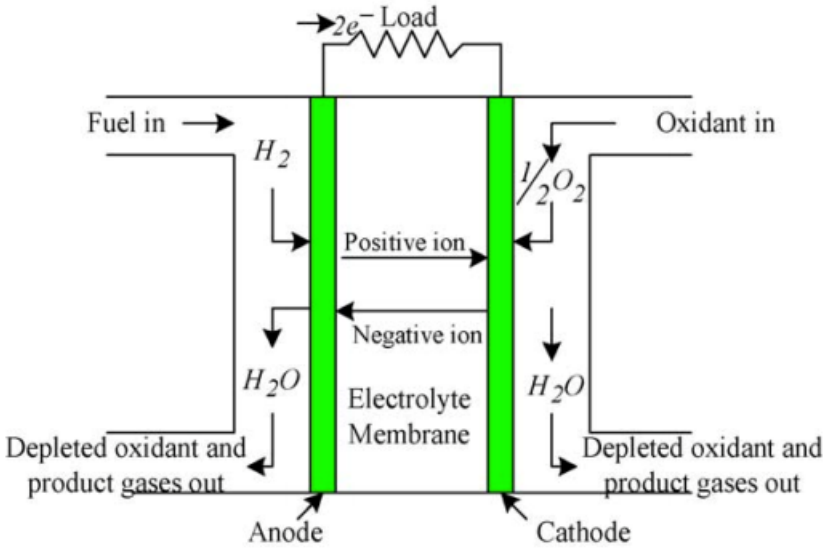

Fig. 1-1. A schematic image of a unite cell

- Fuel cell stacking

  In order to meet the requirement for the applications, unit cells must be connected in series into a cell stack via electrically conductive interconnects such as bipolar plate to improve the voltage and current output level as shown in Fig. 1-2.

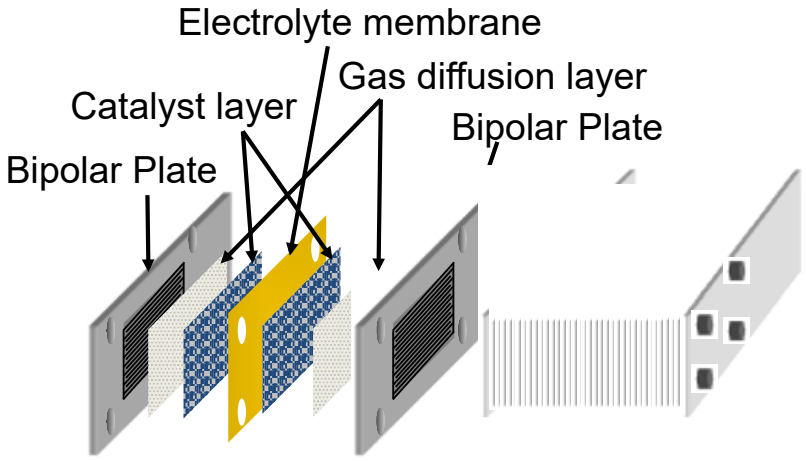

Fig. 1-2 Fuel cell stack

- Fuel cell systems

  In addition to the stack, there are other components such as fuel processing system, air management system and power conditioning system, the so-called balance of plant (BoP). The Bop forms the fuel cell system together with the stack.

1.1.2 Fuel cell types

A variety of fuel cells are developed in difference stages with distinct characteristics and classified according to the nature of the electrolyte and fuel used [9]. The type of electrolyte decides the operating temperature range, the kind of need catalyst used to speed up the reactions at the electrodes and the kind of chemical reaction. The available five major different types are:

- Polymer electrolyte fuel cell (PEFC)

  The PEFC consists of a solid polymer electrolyte that is an excellent proton

conductor. Water is the only liquid in the fuel cell. The PEFC is operated at low temperatures around 80℃. The low enough temperature and higher power density makes them suitable for homes and cars. However, the drawbacks are that the platinum catalyst used on both the anode and cathode and the purified fuels raise costs [10].

- Alkaline fuel cells (AFC)

  The AFC generally use an alkaline solution such as potassium hydroxide (KOH) in water as their electrolyte. The AFC has the capability to reach about 70 percent efficiency. It operates at temperature between 140 to 200℃. The AFCs require pure hydrogen and oxygen due to their susceptibility to carbon contamination [11]. The one disadvantages of it is that the corrosive electrolyte has shorter life span. Because of the flexible usage of a wide range of electro-catalysts, the excellent performance on hydrogen and oxygen make it an advantage.

- Phosphoric acid fuel cell (PAFC)

  The phosphoric acid fuel cell (PAFC) is a type of fuel cell that uses a liquid phosphoric acid in a bonded silicon carbide matrix as the electrolyte. The operating temperature of it is about 180℃. The electrical efficiency is relatively low, ranges from 40 to 80 percent. The low power density and durability issues limited the commercial success of the PAFC. When the pure hydrogen (H_2) is used as its input fuel, the involved chemical reaction in PAFC is same as that of PEFC [12]. PAFC technology has the additional

advantage that it is more tolerant to impurities, in particular reformed hydrocarbon fuels compared to the PEFC and AFC.

- Molten carbonate fuel cell (MCFC)

  The Molten carbonate fuel cells (MCFC) usually use high temperature compounds as the electrolyte which is molten carbonates salt suspended in a porous ceramic matrix. The MCFC operates at about 650℃. Efficiency is in a range of 60 to 80 percent. The development of the MCFC stems from the problem of corrosive and mobile electrolyte, which lead to the requirement of high-cost nickel and high-grade stainless steel [13,14].

- Solid oxide fuel cell (SOFC)

  The electrolyte in solid oxide fuel cell is a hard solid ceramic, such as stabilized zirconium oxide. The operating temperatures of it is very high, about 800-1000℃. The high efficiency of 50-60 percent [15] and no need a separate reformer are the main advantages. However, mechanical vulnerability and high cost have limited the application of SOFC [16].

The summary of major differences of the fuel cell types is shown in Table 1-1[5].

Table 1-1 Summary of major of major differences of the fuel cell types [5]

	PEFC	AFC	PAFC	MCFC	SOFC
Electrolyte	Hydrated Polymeric Ion Exchange Membranes	Mobilized or Immobilized Potassium Hydroxide in asbestos matrix	Immobilized Liquid Phosphoric Acid in SiC	Immobilized Liquid Molten Carbonate in $LiAlO_2$	Perovskites (Ceramics)
Electrodes	Carbon	Transition metals	Carbon	Nickel and Nickel Oxide	Perovskite and perovskite / metal cermet
Catalyst	Platinum	Platinum	Platinum	Electrode material	Electrode material
Interconnect	Carbon or metal	Metal	Graphite	Stainless steel or Nickel	Nickel, ceramic, or steel
Operating Temperature	40 – 80 °C	65°C – 220 °C	205 °C	650 °C	600-1000 °C
Charge Carrier	H^+	OH^-	H^+	$CO3^=$	$O^=$
External Reformer for hydrocarbon fuels	Yes	Yes	Yes	No, for some fuels	No, for some fuels and cell designs
External shift conversion of CO to hydrogen	Yes, plus purification to remove trace CO	Yes, plus purification to remove CO and CO_2	Yes	No	No
Prime Cell Components	Carbon-based	Carbon-based	Graphite-based	Stainless-based	Ceramic
Product Water Management	Evaporative	Evaporative	Evaporative	Gaseous Product	Gaseous Product
Product Heat Management	Process Gas + Liquid Cooling Medium	Process Gas + Electrolyte Circulation	Process Gas + Liquid cooling medium or steam generation	Internal Reforming + Process Gas	Internal Reforming + Process Gas

1.2 Polymer electrolyte Fuel cells (PEFCs)

1.2.1 Overview

Polymer electrolyte fuel cells (PEFCs) that use a polymer membrane as an electrolyte are able to operate at low temperatures, generate high power densities and good energy efficiency [17]. Thereby, these advantages allow it can be made smaller making increasingly attractive for transport applications as well as for certain portable and vehicle applications. The PEFC is one of the most promising clean energy converters without generating carbon dioxide emissions.

1.2.2 Cell components

A basic schematic of PEFC is shown in Fig. 1-3. Typical PEFC components include:

- Two electrodes (anode and cathode)
- Proton exchange membrane (PEM)
- Gas diffusion layer (GDL)
- Catalyst
- Bipolar plate

The electrochemical reactions occur at two electrodes. Reactant hydrogen gas is fed to the anode of the fuel cell that is oxidized into protons, while oxygen (air) gas is fed to the cathode of the fuel cell that is reduced to water. Two electrodes is contact with a membrane that is designed to separate the reactants (hydrogen and oxygen/air) and

transit the protons towards the electrodes. Two porous structures, gas diffusion layer (GDL) and an active layer (AL) constitute the electrodes.

The Gas diffusion layer (GDL) connects the catalyst and current collector electrically also as known as bipolar plates, and needs porous, electrically conductive and thin. (GDL) is typically cloth or carbon paper with the thickness around 100-300 μm to help to remove the product water and prevents water flooding in the porous cathode. In addition, the porous GDL in PEFC as the electrical conductor ensures the diffusion of reactants effectively to the catalyst layer and allow the transportation of electrons to and from the catalyst layer.

In the active layer (AL) that composed of the catalyst particles, pore spaces and ionomer compose, a three-phase boundary can be formed. The electrochemical oxidation and reduction reactions occur and protons, reactant gases and electrons meet in this three-phase boundary.

The membrane electrode assembly (MEA) that consists of electrolyte membrane, catalyst layers and gas diffusion layers is the heart of the PEFC [18]. The MEA is sandwiched between anode and cathode electrodes that have the catalyst embedded in them. In each cell, these components are prepared individually and then assembled together at high pressures and temperature to form the MEA [19]. One important features of the MEA is the sealing function to prevent the anode and cathode gas from mixing and leaking to the outside of the fuel cell stack. The property of a MEA is affected by the following factors:

(1) The characteristics of the proton exchange membrane (PEM), catalyst, gas

diffusion layers and so on;

(2) The MEA structure and the way it is manufactured;

(3) The structure of fuel cell stack and the flow field plates;

(4) PEFC operating conditions.

The catalyst material is the platinum (pure or alloyed) [20] for both the anode and cathode, up to now. The hydrogen oxidation reaction (HOR) and oxygen reduction reaction (ORR) can be catalyzed by platinum. However, in a PEFC, the hydrogen oxidation reaction on platinum is very fast, almost three orders of magnitude higher of exchange current density than that of the oxygen reduction reaction. Because of the low kinetics of the ORR, the performance is loss [21,22]. The characteristics of activity, stability, selectivity and poisoning resistance are essential for the PEFC catalyst.

Generally, the proton exchange membrane (PEM) is the core component of a PEFC and plays an important role. The PEM is an electronic insulator that can charge carrier for protons, prevent the electrons form passing through the membrane and separate the hydrogen and oxygen (air) gases [23]. Pure polymer membranes or composite membranes can be made into PEMs. As a benchmark, Nafion developed by Dr. Walther Grot in the late 1960s is the most common PEM used in the fuel cell industry [24]. The Nafion material is highly chemically resistant, mechanically strong, acidic, absorptive to water and good proton conductors. The most widely types of the Nafion membranes used is 112 (2 mil), 115 (5mil), 117 (7 mil) and 1110 (10 mil), where 1 mil=25.4 μm.

Bipolar plate is one of the most important components of PEFC and also the point of this thesis, the description of bipolar plate will be written in next section.

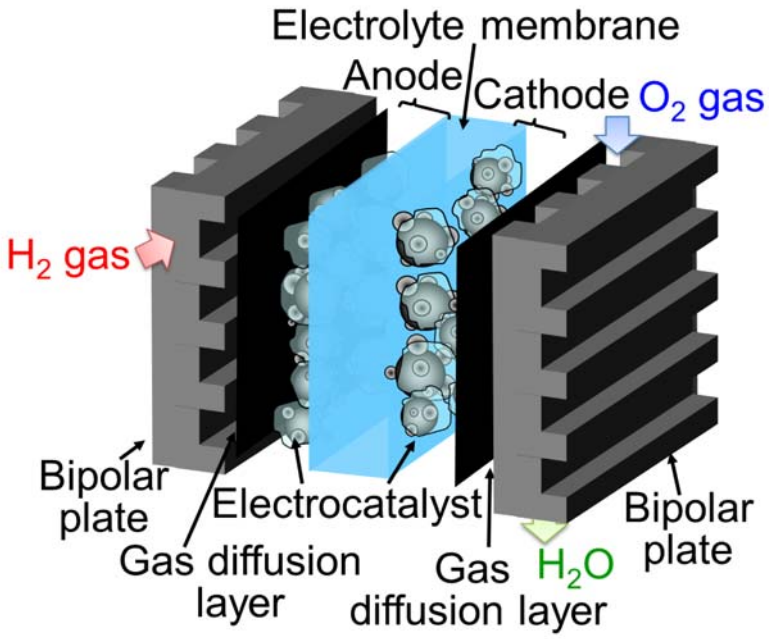

Fig. 1-3. Basic schematic of a PEFC.

1.3 Bipolar plate of PEFCs

1.3.1 Bipolar plate properties

Bipolar plate (BP) is a significant component of the PEFC stack that account for more than 40% cost of the total stack and about 80% weight of the whole PEFC [25]. The bipolar plates have a number of functions in a PEFC stack [26], such as supply the hydrogen and oxygen gases to the active areas, facilitate heat and water management, provide structure support for the whole PEFC and bring current away from one individual cell to another individual cell [27]. The bipolar plates are primarily designed to offer the reactions gases (hydrogen and oxygen) via flow channels to the anode and cathode electrodes. The different types of the flow channels are shown in Fig. 1-4 [28].

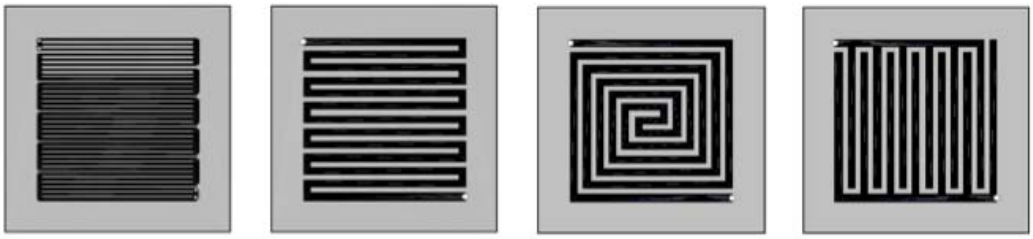

(a) (b) (c) (d)

Fig. 1-4. Bipolar plates with different channel designs [28].

(a) GlobeTech geometry; (b) Serpentine geometry; (c) Spiral geometry;

(d) Discontinuous channels geometry

There are many requirements for bipolar plates as follows [29,30]:

- Low cost material
- Reasonable thermal stability and high thermal conductivity (>10 W / mK)
- Good Electrical conductivity (in-plane <0.01 Ω cm^2)
- Gas flow easily
- Low permeability to hydrogen/ gas (<10^{-4} cm^3 / s cm^2)
- High manufacturability
- Reasonable compressive strength
- Low volume and weight
- High corrosion resistance and chemical stability
- Low interfacial contact resistance (<20 mΩ cm^2 at 150 N cm^{-2})
- Density (<5 g cm^{-3})
- Corrosion rate (<1 μA cm^{-2})
- Tensile strength (> 41 MPa)
- Flexural strength (>59 MPa)

1.3.2 Bipolar plate classification

So far, the materials used as bipolar plates can be classified as [31]:

1. Non-metal

   Non-porous graphite plates

2. Metals

   (1) Non-coated

   Austenitic stainless steel; Ferritic stainless steel

   (2) Coated

   Bases: aluminum; titanium; nickel; stainless steel

   Coatings: graphite; conductive polymer; diamond-like carbon; organic self-assembled monopolymers; noble metals; metal carbides; metal nitrides

3. Polymer composite plates

   (1) Metal based

   porous graphite; polycarbonate plastic; stainless steel

   (2) Carbon based

   Resin: poly (vinylidene fluoride); polypropylene; polyethylene; epoxy resin; phenolic resins; furan resin; vinyl ester

   Filler: carbon/graphite; carbon black; coke-graphite

   Fiber: carbon/graphite; cellulose; cotton flock

The advantages and disadvantages of different types of bipolar plate materials are shown in Table 1-2 [32].

Table 1-2 The advantages and disadvantages of different types of bipolar plate materials [32]

Material	Advantages	Disadvantages
Graphite	Excellent corrosion resistance Low bulk resistivity Low contact resistance	Poor mechanical properties (brittleness) Porosity High weight and volume High processing cost
Carbon-carbon composites	Low density High corrosion resistance Low contact resistance	Low mechanical strength Low bulk electrical conductivity High price
Carbon-polymer composites	Low cost Good corrosion resistance Low weight No machining process Commercial availability of the raw materials	Low mechanical strength Low electrical conductivity
Metal	Good electrical conductivity High thermal conductivity Low cost Excellent mechanical properties Ease of fabrication Small volume	Severe corrosion (membrane poisoning and formation of insulating surface oxide)

1.3.3 Graphitic bipolar plate

Generally, bipolar plate is divided into carbon-based and metallic based. Graphite, the standard carbon-based bipolar plate is the commonly used bipolar plate material due to the excellent chemical property, resistance to corrosion and high conductivity in the PEFC operating environment. However, the high cost of production of gas channels in the surface of the graphite bipolar plate is one of the main problems that

limit the use of the graphite bipolar plate. The graphite also has poor mechanical properties and inherent brittleness [33] that is not suitable for mobile and transportation applications need effective mass production [34]. In order to make the graphite impermeable to the oxygen and fuel, graphite bipolar plate have to be coated. In additional, the molecular structure, flexural strength and porosity have limited the thickness of graphite bipolar plate to about 4-6 mm [35,36] resulting in low power density, high weight and volume. Therefore, the disadvantages of graphite bipolar plate have led many researchers to make effort to develop other materials to replace it that can meet the requirements of the bipolar plate.

Graphite composite materials are more suitable for bipolar plates than graphite that can improve fabrication technologies of bipolar plates and reduce the cost. The commercially available polymers and conductive carbon compounds comprise the composite materials. However, the graphite composite materials exhibit low electrical conductivity [37].

1.3.4 Metallic bipolar plate

Metallic bipolar plates are alternative to graphite and attracting more attention of fuel cell researchers in recent years due to good electrical conductivity, low cost, high formability, superior mechanical properties, high manufacturability and low gas permeation rates [38,39]. Metals also have advantages over graphite bipolar plates such as high modulus, strength, toughness and unique mechanical properties that can

be made thinner to reduce volume and weight of PEFC. Different types of metals and alloys have been considered as bipolar plates. Aluminium, titanium and stainless steels have high gas impermeability, excellent mechanical properties and suitable for industrial production. In the low PH values polymer electrolyte fuel cell environment, the metals are very stable.

However, metals are more susceptible to corrosion that can occur at the anode as it does at the cathode of an acid PEFC environment. At the anode, the oxide protective metal layer can be reduced in the reducing environment, leading to hydride formation and dissolution of the metal in product water. At the cathode, the metal oxide layers can grow because of the air and positive potentials. The growth of the oxide layers lead to the increase of electrical resistance. Therefore, the activity of an electrode catalyst can be reduced. In addition, the polymer electrolyte membrane can be contaminated by the metal dissolution.

In fact, most of the researchers have focused on the work of austenitic stainless steel contains of nickel and chromium elements to replace graphite used as bipolar plate for PEFC and SS 316 and SS 316L has been chosen frequently. Although the SS 316 stainless steel offers good mechanical properties, corrosion resistance and relatively low cost, Lin et al. [40] found that the interfacial contact resistance (ICR) of SS 316 is about 16 times higher than that of the Department of Energy target that cannot meet the desirable fuel cell performance. Other austenitic stainless steels such as SS 304 [41] and ferritic stainless steel such as AISI446 [42] have been also investigated as the candidate bipolar plate materials.

In order to solve the corrosion problem and improve the performance of metallic stainless steel bipolar plate, surface treatment techniques are required to increase the corrosion property and decrease the interfacial contact resistance. The most widely used surface treatment techniques for metallic bipolar plates are surface coating and nitriding treatment.

1.4 Surface treatment technique of metallic Bipolar plate

1.4.1 Surface coating

Because that the metallic bipolar plates can be corroded in the fuel cell environment which cause an increase of interfacial contact resistance (ICR), surface modification is necessary for metallic bipolar plates. Coating technique can be applied on the stainless steels for protection to improve the properties of PEFC when operating in an acidic environment [43].

The coating methods for the metallic bipolar plates include [44]:

(1) Physical vapor deposition (PVD) techniques;

(2) Sputtering and glow discharge decomposition;

(3) Chemical vapor deposition (CVD) technique;

(4) Liquid phase chemical techniques;

(5) Chemical anodization/oxidation overcoating;

(6) Painting

Many of these coating methods have been investigated. Silva et al. evaluated interfacial contact resistance (ICR) and corrosion resistance of Ni-based alloys, different types of stainless steels and nitride coated steels as metallic bipolar plates in PEFC environment and reported that only nitride-coated SS 304 stainless steels show low interfacial contact resistance (ICR) and good corrosion resistance [45]. The metallic bipolar plate can also be coated with conducting polymer polypyrrole (PPY) and polyaniline (PANI) to prevent bipolar plates from corrosion under PEFC fuel cell

conditions and keep contact resistance at acceptable value [46].

However, due to pinhole defects, conventional coating techniques for metallic bipolar plates may increase the corrosion rate and have not been proven sufficiently. The pinhole defects may result in metallic ion contamination of the membrane and cause local corrosion. Recently, nitriding treatment is alternative to coating treatment for metallic bipolar plates [47] and there is no pinhole defects problem for the nitriding treatment.

1.4.2 Nitriding process

The metallic bipolar plates may suffer from corrosion and form passive layers on their surface when contact with the acidic PEFC environment co-existing with oxygen and product water at high temperature. The formed passive layer has high electrical resistance and is electrically semiconductor that can degrade the power output of PEFC stacks [48]. In order to enhance the performance of metallic bipolar plates in the PEFC and obtain the defect-free, protective and conductive coatings, nitriding treatment can be used.

Nitriding technique is a heat-treating process that diffuses nitrogen into the surface of the base metal to form modified protective surface layers. The three main nitriding methods are gas nitriding, plasma nitriding and salt bath nitriding, the former two nitriding methods are commonly used for metallic bipolar plates in PEFC [49,50]. The gas nitriding is carried out in nitrogen rich gases atmosphere such as nitrogen gas (N_2) and ammonia (NH_3) at different temperatures. Plasma nitriding known as plasma

ion nitriding, ion nitriding or glow-discharge nitriding is an industrial operation surface treatment. The reactivity of the nitriding media in plasma nitriding is decided by the gas ionized state not the temperature. The nitrided layers containing nitrides is formed through chemical reaction at the metal surface, not a deposited coating. The nitrides are corrosion resistant with low surface contact resistance.

Wang et al. [49] carried out thermal nitridation in pure nitrogen of a Ni-50Cr alloy and found the formation of a protective, dense and continuous surface layer. The results show that the interfacial contact conductivity and corrosion resistance of nitrided Ni-50Cr alloy are significantly improved. Lin et al. [51] used active screen plasma nitriding (ASPN) to modify the surface of austenitic 316 stainless steel used as bipolar plates in PEFC. The results reveal that the interfacial contact resistance (ICR) can be decreased and the corrosion resistance can be improved after ASPN treatment because of the formation of nitrogen supersaturated S-phase layer.

During the high nitriding temperature, the N_2 gas can react with the metal in the stainless steel resulting in the formation of the metal nitrides such as Cr-N [49, 50]. The CrN thin films reveal semiconducting behavior of electrical resistivity that can be strongly influenced by the parameters of preparation [52].

The nitriding treatment has been proved an effective way to improve the performance of metallic bipolar plate in PEFC.

1.5 Purpose of this thesis

As a strong contender for alternative power sources, the polymer electrolyte fuel cell (PEFC) that converts the chemical energy of the reactant into electrical energy is one of the most promising clean energy converters in the coming years. As we all know, the bipolar plate is a key component of the PEFC. Two types of bipolar plates, carbon-based (graphite) and metallic-based (stainless steel) are commercially available. However, there are many disadvantages for graphite to be used, such as brittleness, lack of mechanical strength, high permeability and high manufacture cost. The metallic bipolar plates are alternative to the graphite bipolar plates due to excellent mechanical properties, good electrical and thermal conductivity, low volume and cheaper material cost. However, one big problem of the metallic bipolar plates is the corrosion in the actual cell environment. Now the high cost of PEFC is a big challenge before the PEFC application can be commercialized and the bipolar plates account for about 21%. Because that nickel is very expensive, in this work, in order to decrease the cost of PEFC and improve the corrosion resistance of metallic bipolar plates, we investigate corrosion behavior of Ni-free inexpensive stainless steel used for bipolar plates in PEFC with and without nitriding heat treatment.

References

[1] E. A. Merewether, Alternative sources of energy-an introduction to fuel cells, 2003, 1.

[2] C. Rayment, S. Sherwin, Introduction to fuel cell technology, 2003, 11.

[3] E. I. Ortiz-Rivera, A. L. Reyes-Hernandez, R. A. Febo, Understanding the history of fuel cell, IEEE Conference on the History of Electric Power, 2007, 117.

[4] A. B. Stambouli, E. Traversa, Fuel cell, an alternative to standard sources of energy, Renewable and Sustainable Energy Reviews, 6 (2002), 297-306.

[5] EG&G Technical Services, Inc, Fuel Cell Handbook (Seventh Edition), 2004, 1-1~1-6.

[6] X. Huang, Z. Zhang, J. Jiang, Fuel cell technology for distributed: an overview, IEEE Symposium on Industrial Electron, 2006, 1613-1618.

[7] A. Kirubakaran, S. Jain, R. K. Nema, A review on fuel cell technologies and power electronic, Renewable and Sustainable Energy Reviews, 13 (2009), 2430-2440.

[8] P. K. Shah, Introduction to Fuel Cells, 2007, P. 1.

[9] L. V. Biert, M. Godjevac, K. Visser, P. V. Aravind, A review of fuel cell systems for maritime applications, J. Power Sources, 327 (2006), 345-364.

[10] Y. Wang, K. S. Chen, J. Mishler, S. C. Cho, X. C. Adroher, A review of polymer electrolyte membrane fuel cells: Technology, application, and needs on fundamental research, Appl. Energy, 88 (4) (2011), 981-1007.

[11] T. E. Lipmann, Manufacturing and lifecycle costs of battery electric vehicles,

direct-hydrogen fuel cell vehicles, and direct-methanol fuel cell vehicles, Energy Conversion Engineering Conference and Exhibit, (IECEC) 35th Intersociety, (2000), 1352-1358.

[12] M. Farooque, H. C. Maru, Fuel cells-the clean and efficient power generators, Proceeding of the IEEE, 89 (2001), 1819-29.

[13] J. P. P Huijsmans, G. J. Kraaij, R. C. Makkus, G. Rietveld, E. F. Sitters, H. T. J. Reijers, An analysis of endurance issues for MCFC, J. Power Sources, 86 (1) (2000), 117-121.

[14] A. Kulkarni, S. Giddey, Materials issues and recent developments in molten carbonate fuel cells, J. Solid State Electrochem., 16 (10) (2012), 3123-3146.

[15] R. T. Leah, A. Bone, A. Selcuk, D. Corcoran, M. Lankin, Z. Dehaney-Steven, M. Selby, Development of highly robust, volume-manufacturable metal-supported sofcs for operation below 600°, P. Whalen, ECS Trans., 35 (1) (2011), 351-367.

[16] S. Pellegrino, A. Lanzini, P. Leone, Techno-economic and policy requirements for the market-entry of the fuel cell micro-CHP system in the residential sector, Appl. Energy, 143 (2015), 370-382.

[17] K. H. Choi, H. S. Kim and T. H. Lee, Electrode fabrication for proton exchange membrane fuel cells by pulse electrodeposition, J. Power Sources, 75 (1998), 230-235.

[18] S. Litster, G. McLean, FEM Fuel cell electrodes, J. Power Sources, 130 (2004), 61-76.

[19] D. Ye, Z. Zhan, A review on the sealing structures of membrane electrode assembly of proton exchange membrane fuel cells, J. Power Sources, 231 (2013), 285-292.

[20] N. Yousfi-Steiner, Ph. Mocoteguy, D. Candusso and D. Hissel, A review on polymer electrolyte membrane fuel cell catalyst degradation and starvation issues: causes, consequences and diagnostic for mitigation. J. Power Sources, 194 (2009), 130-145.

[21] O. T. Holton and J. W. Stevenson, The Role of Platinum in Proton Exchange Membrane Fuel Cells, Platinum Metals Rev., 57 (4) (2013), 259-271.

[22] C. He, S. Desai, G. Brown and S. Bollepalli, PEM fuel cell catalysts: cost, performance, and durability, Electrochemical Society Interface, 14 (3) (2005), 41-44.

[23] S. J. Peighambardoust, S. Rowshanzamir, M. Amjadi, Review of the proton exchange membranes for fuel cell applications, Int Journal Hydrogen Energy, 35 (2010), 9349-9384.

[24] A. Kraytsberg, Y. Ein-Eli, Review of advanced materials for proton exchange membrane fuel cells, Energy and Fuels, 28 (2014), 7303-7330.

[25] H. Tsuchiya, O. Kobayashi, Mass production cost of PEM fuel cell by learning curve, Int Journal Hydrogen Energy, 29 (2004), 985-990.

[26] J. Cui, B. Jing, X. Xu, L. Wang, F. Cheng, S. Li, Z. Wen, S. Ji and J. Sun, Performance of niobium nitride-modified AISI316L stainless steel as bipolar plates for direct formic acid fuel cells, Int Journal Hydrogen Energy,

http://dx.doi.org/10.1016/j.ijhydene.2017.02.145.

[27] A. Hermann, T. Chaudhuri and P. Spagnol, Bipolar plates for PEM fuel cells: A review, Int Journal Hydrogen Energy, 30 (2005), 1297-1302.

[28] T. Mennola, Cathode Flow Field Geometry in a PEMFC, Laboratory of Advanced Energy Systems, Helsinki University of Technology, Finland, http://www.tkk.fi/Units/AES/papers/papers/mennola01a.pdf.

[29] R. A. Antunes, M. C. L. Oliveira, G. Ett and V. Ett, Corrosion of metal bipolar plate for PEM fuel cells: A review, Int Journal Hydrogen Energy, 35 (2010), 3632-3647.

[30] S. Karimi, N. Fraser, B. Roberts and F. R. Foulkes, A Review of Metallic Bipolar Plates for Proton Exchange Membrane Fuel Cells: Materials and Fabrication Methods, Adv. Mater. Sci. Eng., (2012), 1-22.

[31] A. Hermann, T. Chaudhuri and P. Spagnol, Bipolar plates for PEM fuel cells: a review, Int Journal Hydrogen Energy, 30 (2005), 1297-1302.

[32] X. Z. Yuan, H. Wang, J. Zhang, D. P. Wilkinson, Bipolar plates for PEM fuel cells-from materials to processing, J. New. Mat. Electrochem. Systems, 8 (2005), 257-267.

[33] G. O. Mepsted and J. M. Moore, Performance and durability of bipolar plate materials, in handbook of fuel cells-fundamentals, technology and applications, (2003), 286-293.

[34] H. Tsuchiya and O. Kobayashi, Mass production cost of PEM fuel cell by

learning curve, Int Journal Hydrogen Energy, 29 (2004), 985-990.

[35] B. Cunningham, The development of compression moldable polymer composite bipolar plates for fuel cells [Ph.D. dissertation], Virginia Polytechnic Institute and State University, 2007.

[36] K. RoBerg and V. Trapp, Graphite-based bipolar plates, in handbook of fuel cells fundamentals, technology and applications, (2003), 308-314.

[37] K. Kang, S. Park, A. Jo, K. Lee and H. Ju, Development of ultralight and thin bipolar plates using epoxy-carbon fiber prepregs and graphite composites, Int Journal Hydrogen Energy, 42 (2017), 1691-1697.

[38] Y. Hung, H. Tawfik, and D. Mahajan, Durability and characterization studies of polymer electrolyte membrane fuel cell's coated aluminum bipolar plates and membrane electrode assembly, J. Power Sources, 186 (2009),123-127.

[39] J. Andre, L. Antoni, and J. P. Petit, Corrosion resistance of stainless steel bipolar plates in a PEFC environment: a comprehensive study, Int Journal Hydrogen Energy, 35 (2010), 3684-3697.

[40] K. Lin, X. Li, L. Tian and H. Dong, Active screen plasma surface co-alloying treatments of 316 stainless steel with nitrogen and silver for fuel cell bipolar plates, Surface &Coatings Technology, 283 (2015), 122-128.

[41] D. P. Davies, P. L. Adcock, M. Turpin and S. J. Rowen, Bipolar plate materials for solid polymer fuel cells, J. Appl. Electrochem., 30 (2000) 101-105.

[42] H. Wang, J. A. Turner, Ferritic stainless steels as bipolar plate material for

polymer electrolyte membrane fuel cells, J. Power Sources, 128 (2004),193-200.

[43] N. F. Asri, T. Husaini, A. B. Sulong, E. H. Majlan and W. R. W. Daud, Coating of stainless steel and titanium bipolar plates for anticorrosion in PEMFC: a review, Int Journal Hydrogen Energy, http://doi.org/10.1016/j.ijhydene.2016.06.241.

[44] V. Mehta, J. S. Cooper, Review and analysis of PEM fuel cell design and manufacturing, J. Power Sources, 114 (2003), 32-53.

[45] R. F. Silva, D. Franchi, A. Leone, L. Pilloni, A. Masci and A. Pozio. Surface conductivity and stability of metallic bipolar plate materials for polymer electrolyte fuel cells, Electrochim Acta, 51 (2006), 3592-3598.

[46] S. Joseph, J. McClure, R. Chianelli, P. Pich and P. Sebastian. Conducting polymer-coated stainless steel bipolar plates for proton exchange membrane fuel cells (PEMFC), Int Journal Hydrogen Energy, 30 (2005), 1339-1344.

[47] M. P. Brady, K. Weisbrod, I. Paulauskas, R. A. Buchanan, K. L. More, H. Wang, M. Wilson, F. Garzon and L. R. Walker, Preferential thermal nitridation to form pin-hole free Cr-nitrides to protect proton exchange membrane fuel cell metallic bipolar plates, Scripta Mater. 50 (2004), 1017-1022.

[48] R. J. Tian, J. C. Sun and L. Wang, Effect of plasma nitriding on behavior of austenitic stainless steel 304L bipolar plate in proton exchange membrane fuel cell, J. Power Sources, 163 (2007), 719-724.

[49] H. Wang, M. P. Brady, G. Teeter and J. A. Turner, Thermally nitrided stainless steels for polymer electrolyte membrane fuel cell bipolar plates, Part 1: Model Ni-50Cr

and austenitic 349^{TM} alloys, J. Power Sources, 138 (2004), 86-93.

[50] Y. Yu, S. Shironita, T. Mizukami, K. Nakatsuyama, K. Souma, M. Umeda, Corrosion-resistant characteristics of nitrided Ni-free stainless steel for bipolar plate of polymer electrolyte fuel cell, Int. J. Hydrogen Energy, 42 (2017), 6303-6309.

[51] K. Lin, X. Li, Y. Sun, X. Luo and H. Dong. Active screen plasma nitriding of 316 stainless steel for the application of bipolar plates in proton exchange membrane fuel cells, Int J Hydrogen Energy, 39 (2014), 21470-21479.

[52] I. Batko, M. Batkova, F. Lofaj, Electrical resistivity of CrN thin films, Acta Physica Polonica A, 125 (2014), 415-416.

Chapter 2 Effect of Cr content on the corrosion resistance of Ni-free stainless steels as bipolar plate of PEFC

2.1 Introduction

The polymer electrolyte fuel cell (PEFC) that converts the chemical energy of the reactants into electrical energy has received significant attention for use in fuel cell vehicles and stationary applications [1]. However, the practical operating voltage from a single cell cannot meet the requirement of application. Therefore, bipolar plates are used to connect the cells in series. In recent years, due to high electrical conductivity, manufacturability, gas impermeability and superior mechanical properties, as an alternative material, metallic bipolar plates such as stainless steel have been attracting the attention of the researchers used for bipolar pate in PEFC [2].

Stainless steels are increasingly used in construction and structural applications because of the attractive appearance, corrosion resistance, good strength and fatigue properties [3,4,5]. In recent years, as an inexpensive alloys, the ferritic stainless steels attract more and more attention due to the absence of nickel [6,7]. The ferritic stainless steels were adopted to use in the manufacture of engine mufflers, nuts, bolts and heat resistant tools [8]. In some case, the need of good corrosion resistance and wear resistance when used in aggressive environments has limited the application of the ferritic stainless steel such as the bipolar plate in polymer electrolyte fuel cells (PEFCs) [9].

Ferritic stainless steel SUS445 was developed specifically for architectural applications and has been used in Japan since 1993. The extra high content of the corrosion-resisting element, chromium (22.1%) and added molybdenum give it some big technical benefits over other stainless steels, such as SUS430 and SUS316 stainless steels [10]. However, the H_2SO_4 solution can corrode the SUS445 stainless steel and deteriorate its working life.

In this study, the special Cr-rich stainless steel with higher Cr content (24 %) compared to that of SUS445 stainless steel was prepared. The effect of Cr content on the corrosion resistance of Ni-free stainless steels as bipolar plate of PEFC was investigated. The corrosion behavior of 4 types Ni-free stainless steels with different Cr contents was measured using linear sweep voltammetry (LSV). The surface composition, phase structure, surface morphology and surface electrical conductivity of the 4 types stainless steels were characterized by glow discharge optical emission spectroscopy (GD-OES, Horiba GD-Profiler 2), X-ray diffraction (XRD), scanning electron microscopy (SEM) and four-point probe resistivity measurements.

2.2 Experimental

2.2.1 Material

The 4 types Ni-free stainless steels used in this study were SUS410, SUS430, SUS445 and Cr-rich. The chemical compositions (mass %) of these four types stainless steels are shown in Table 2-1. The Cr-rich stainless steel was specially prepared for this experiment. The SUS445 stainless steel contains small amounts of aluminum (Al), molybdenum (Mo), titanium (Ti) and niobium (Nb) elements compared to other stainless steels. All the 4 types stainless steels are absence of nickel element and contain different Cr contents. The dimensions of the four types stainless steels used in this study are shown in Fig. 2-1.

Table 2-1. The composition of the SUS410, SUS430, SUS445 and Cr-rich stainless steels (mass%).

Sample	Fe	C	Si	Mn	Cr	Mo	Nb	Ti	Al	Ni
SUS410[a]	Bal.	≤0.15	≤0.50	≤1.0	11.5~13.0	–	–	–	–	–
SUS430[a]	Bal.	≤0.12	≤0.75	≤1.0	16.0~18.0	–	–	–	–	–
SUS445[b]	Bal.	0.01	0.18	0.20	22.10	1.20	0.23	0.19	0.09	–
Cr-rich[c]	Bal.	0.05	0.15	0.30	24.0	–	–	–	0.15	–

[a] From The Nilaco Corporation Co., Ltd.

[b] From Nisshin Steel Co., Ltd.

[c] From Hitachi Metals, Ltd.

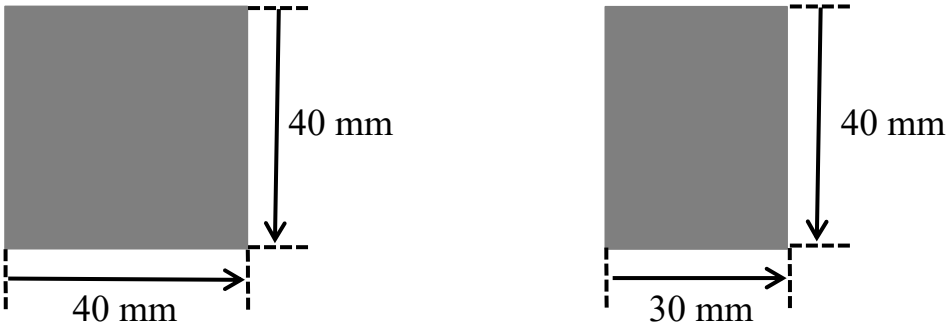

(a) SUS410 (Thickness: 3.9 mm) (b) SUS445 (Thickness: 0.1 mm)

SUS430 (Thickness: 1 mm) Cr-rich (Thickness: 0.1 mm)

Fig. 2-1. Dimensions of the four types stainless steels.

(a) SUS410 and SUS430; (b) SUS445 and Cr-rich.

2.2.2 Surface composition

In order to investigate the depth profiles of the elements on the surface of the 4 types stainless steels, glow discharge optical emission spectroscopy (GDS) was carried out using a Horiba GD-Profiler 2 instrument (Fig. 2-2). GDS is a spectroscopic method to measure depth profiles of constituent elements in solid materials by detecting emissions from atoms accommodated in plasma by sputtering [11]. All materials include metals, glass, semiconductors, polymers and ceramics can be analyzed at the nanoscale with a good sensitivity and with a depth compositional selectivity [12]. GDOED is often used due to the advantages of simple sample preparation, high sensitivity, short measuring time and so on [13]. The measured elements included Fe, C, N, Cr, Al, etc. In this study, the Cr contents of the four types

stainless steel is the main data need to be analyzed.

Fig. 2-2. Horiba GD-Profiler 2 instrument

Measurement parameters:

Anode diameter: 4 mm

Pre-sputtering time: 10 s

Gas exchange time: 30 s

Background measurement time: 10 s

Depth profile measurement time: 30 s (2.7 μm)

Measurement interval: 0.1 s / point

2.2.3 X-ray diffraction

The X-ray diffraction (XRD) experiments were performed by an XRD-6100 made by SHIMADZU (Fig. 2-3). XRD is a basic and useful tool for the crystal structure analysis of various solids [14]. The measurements were carried out in reflection geometry using Cu Kα radiation (λ = 1.5406 Å) generated at 40 kV and 30 mA; 2θ was scanned from 20° to 110° at the scan rate of 2° min^{-1}.

Fig. 2-3. X-ray diffraction machine (XRD-6100)

2.2.4 Electrochemical measurement

The electrochemical measurements were conducted using the Electrochemical Analyzer Model 802B (ALS/[H] CH Instruments) at room temperature. In order to analyze the corrosion characteristics of the SUS410, SUS430, SUS445 and Cr-rich stainless steel, a corrosion test was conducted using an electrochemical three-electrode cell (Fig. 2-4) with a platinum coil counter electrode, an Ag/Ag_2SO_4 reference electrode, and the stainless steel specimen as the working electrode. All the

potentials in this study were converted to the SHE after the measurements. The electrolyte was a 0.5 mol dm^{-3} H_2SO_4 solution. Before the linear sweep voltammetry (LSV) measurement, the stainless steels were washed with acetone and distilled water for 5 min during sonication, then a 30-min Ar gas bubbling was conducted. Subsequently, the cathodic treatment was carried out at the potential of -0.47 V vs. SHE for 1 min and then kept in the cell under the rest potential for 5 min. During this step, the invisible H_2 gas generated on the surface of the sample was removed by Ar bubbling. For the electrochemical measurement, the potential was scanned from the rest potential to 1.1 V vs. SHE at the scan rate of 0.33 mV s^{-1} [15]. The samples after the electrochemical measurement were carefully removed from the cell and cleaned with ethanol. The corrosion resistance of all the samples was evaluated based on the Japanese Industrial Standards (JIS) G0579: 2007 measurement method [16].

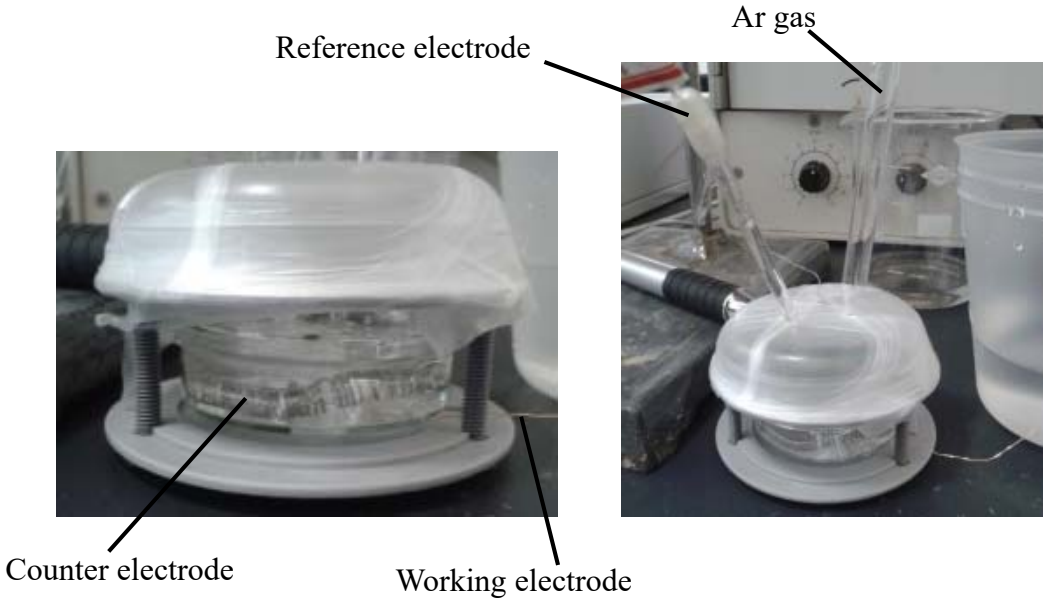

Fig. 2-4. Electrochemical three-electrode cell.

2.2.5 Surface morphology

The scanning electron microscopy (SEM) technique (JSM-6060A, JEOL Ltd.) was used to observe the surface morphology of the stainless steels before and after the LSV measurements stopped at the peak of the polarization curves. The scanning electron microscopy instrument used was shown in Fig. 2-5. Microphotographs of 2000x magnification were obtained at 15 kV.

Fig. 2-5. Scanning electron microscopy instrument (JSM-6060A, JEOL Ltd.).

2.2.6 Electrical conductivity

The electrical conductivity of the bipolar plate is very important, so the electric conductivity of the four types stainless steel was measured with a Mitsubishi Chemical Loresta HP (MCP-T410) electrometer (Fig. 2-6) by using a four-point probe resistivity technique. As a standard measurement, the four-point probe characterization is used to measure the electrical properties of solid and thin films [17].

The surface resistivity Rs is calculated by the equations below:

$$Rs = F*R \tag{2-1}$$

F: resistivity correction factor

R: resistance (Ω □$^{-1}$, □:square)

The measurement parameter of the four-point probe resistivity:

Type of probe: SQUARE

Measured sample shape: RECTANG

Measured sample size: Length (SIZE-X) 40 mm

Width (SIZE-Y) 40 mm for SUS410 and SUS430;

Width (SIZE-Y) 30 mm for SUS445 and Cr-rich

Measured sample thickness: 1 mm for SUS430; 3.9 for SUS410;

0.1 mm for SUS445; 0.1 mm for Cr-rich

Probe distance (POLE-DSTANCE): 1.5 mm

Fig. 2-6. Mitsubishi Chemical Loresta HP (MCP-T410) electrometer.

The resistivity of each stainless steel mentioned in this study is the average data of five measured places that are shown in Fig. 2-7.

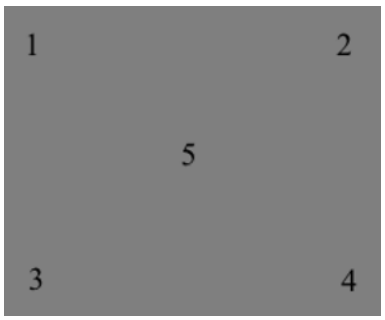

Fig. 2-7. Five measured places of each stainless steel.

2.3 Results and discussion

2.3.1 GDS depth profiles

Figure 2-8 shows the GDS depth profiles of the SUS410, SUS430, SUS445 and Cr-rich stainless steels. The main compositions of these four types stainless steels are Fe and Cr; small amount of C element can be detected. The GDS depth profiles of the SUS410, SUS430, SUS445 and Cr-rich stainless steels show different Cr contents. The depth profiles of Cr element of the SUS410, SUS430, SUS445 and Cr-rich stainless steels are shown in Fig. 2-9. The GDS results show that the Cr contents are increased in the order of SUS410, SUS430, SUS445 and Cr-rich stainless steels. And the Cr-rich stainless steel contains the highest content of the corrosion-resisting element, Cr.

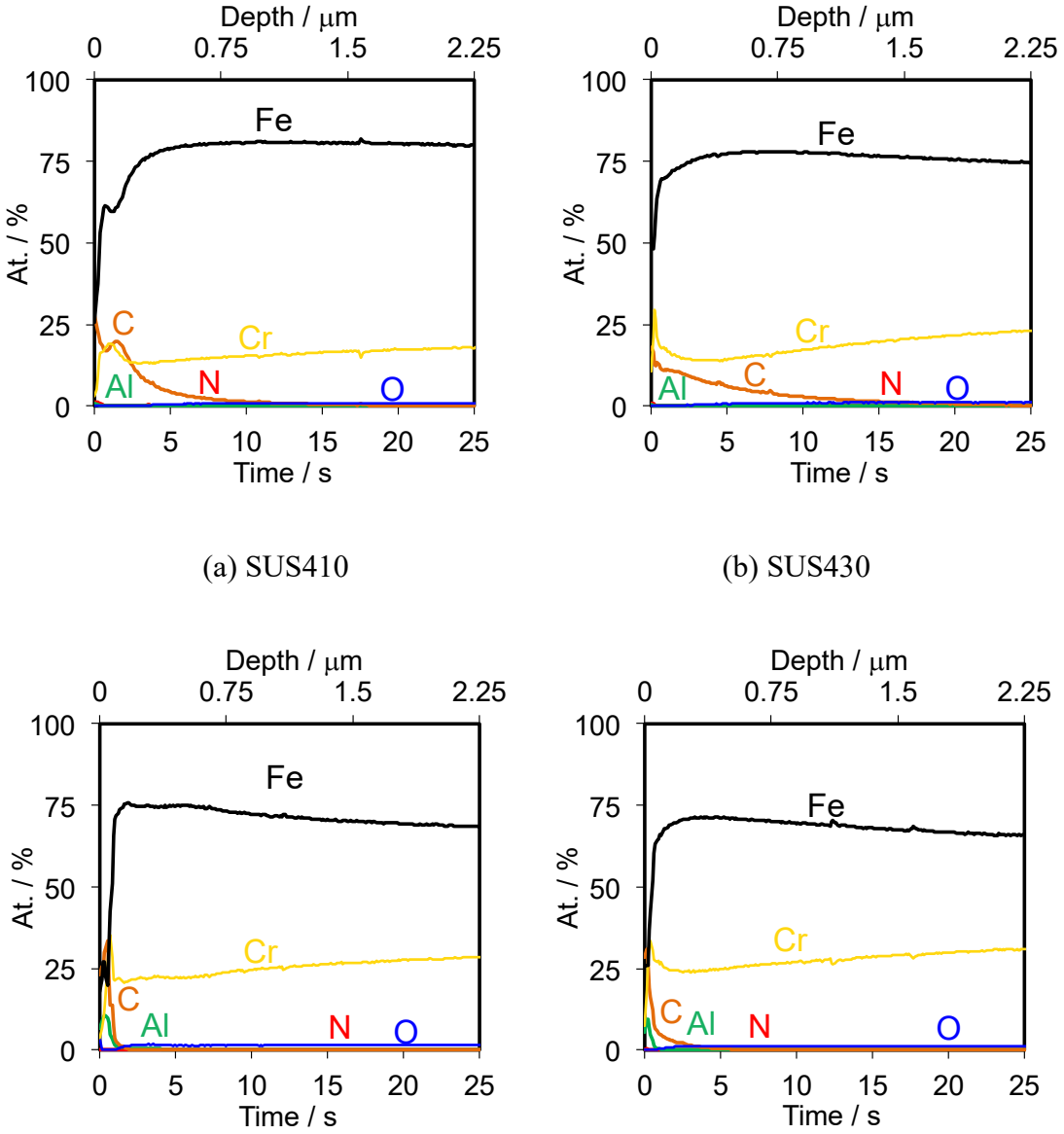

(a) SUS410

(b) SUS430

(c) SUS445

(d) Cr-rich

Fig. 2-8. GDS depth profiles of the SUS410, SUS430, SUS445 and Cr-rich stainless steels.

(a) SUS410; (b) SUS430; (c) SUS445; (d) Cr-rich stainless steel

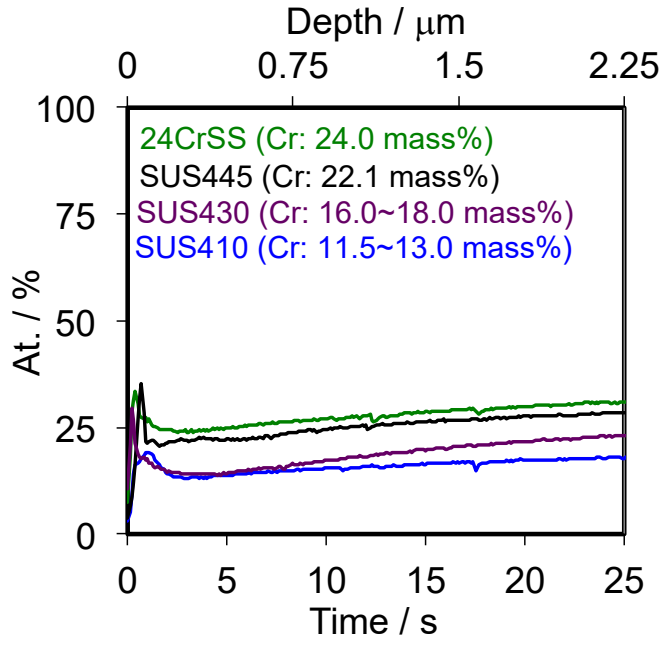

Fig. 2-9. Depth profiles of Cr element of the SUS410, SUS430, SUS445 and Cr-rich stainless steels.

2.3.2 X-ray diffraction analysis

Figure 2-10 shows the XRD patterns of the SUS410, SUS430, SUS445, and Cr-rich stainless steels. The XRD patterns of the all stainless steels show the same diffraction peaks at 44.66°, 64.82°, 82.13° and 98.18°, relative to α-Fe. The XRD results show that the 4 types Ni-free stainless steels are ferritic structure, which is body centred cubic structure (BCC).

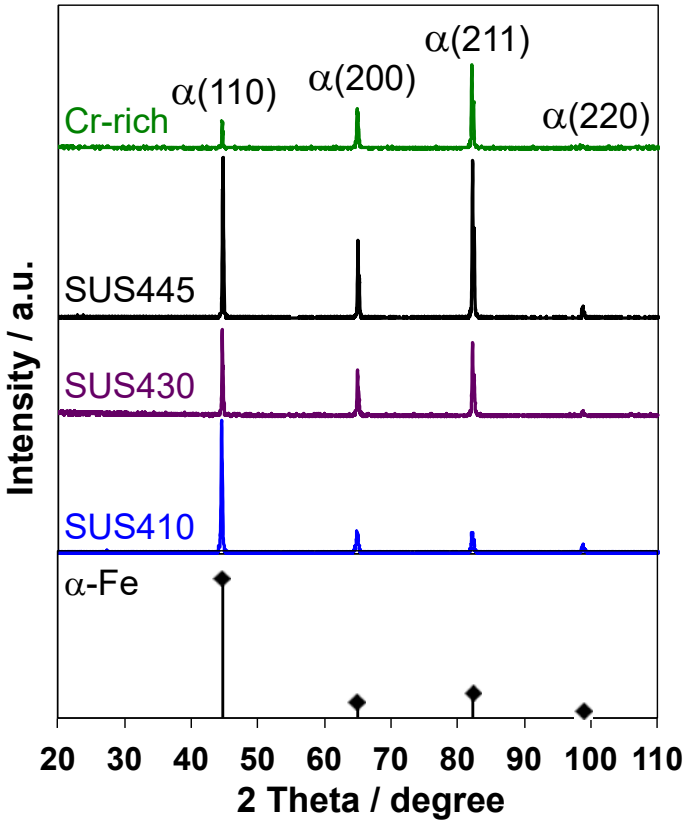

Fig. 2-10. XRD patterns of the SUS410, SUS430, SUS445, and Cr-rich stainless steels.

2.3.3 Corrosion behavior

The polarization curves of the SUS410, SUS430, SUS445 and Cr-rich stainless steels in the Ar-saturated 0.5 mol dm-^{3} H_2SO_4 electrolyte are shown in Fig. 2-11. For the SUS410, SUS430 and SUS445 stainless steels, although the polarization characteristics for these three specimens are almost similar in shape, the polarization curve of the SUS445 stainless steel shows an evident passive region and the lowest current densities in both the active and passive regions due to the high Cr content. The SUS430 stainless steel shows the highest current densities due to the lowest Cr contents.

In the case of the Cr-rich stainless steel, the onset potential shifts toward the positive direction and there is no active current peak compared to the SUS410, SUS430 and SUS445 stainless steel. The current densities of the Cr-rich sample are also decreased indicating a better corrosion resistance of the Cr-rich stainless steel. So the stainless steel contains a higher Cr content, a better corrosion resistance is observed [18].

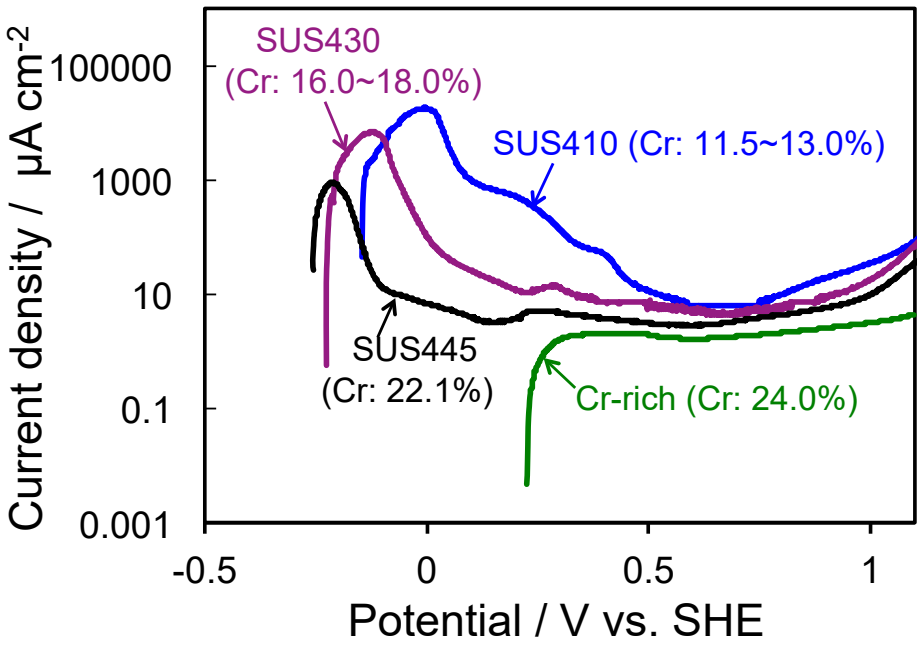

Fig. 2-11. Polarization curves of SUS410, SUS430, SUS445 and Cr-rich stainless steels in Ar-saturated 0.5 mol dm^{-3} H_2SO_4 electrolyte.

2.3.4 Surface morphology

In order to investigate how the corrosion happened on the surface morphology of the 4 types stainless steels, the SEM measurement was carried out to observe the surface morphology of the 4 types stainless steels. Figure 2-12 shows the SEM

images of the 4 types stainless steels before and after LSV measurements stopped at the peak (Fig. 2-13) and the end of the polarization curves. Compared to before LSV measurement (Fig. 2-12(A)), after LSV measurement of the SUS410 stainless steels from rest potential to -0.02 V vs. SHE (Fig. 2-12(B)), we can see clearly that the grain of the SUS410 stainless steel was corroded, so the corrosion was happened on the surface of the SUS410 stainless steel during the active region. For the SUS430 stainless steel, compared to before LSV measurement (Fig. 2-12(D)), after LSV measurement from rest potential to -0.13 V vs. SHE (Fig. 2-12(E)), the surface of the SUS430 stainless steel was corroded during the active region and the grain boundaries became visible due to the chemical attack of the acid solution. Comparing the SEM images of SUS445 stainless steel before (Fig. 2-12(G)) and after LSV measurement from the rest potential to -0.22 V vs. SHE (Fig. 2-12(H)), after LSV measurement, the grain boundaries can be seen but not as clearly as that of the SUS430 stainless steel (Fig. 2-12(E)). The surface of the SUS445 stainless steel was also corroded during the active region. The corrosion damage of the SUS445 stainless steel was less than the SUS430 stainless steel. At the end of LSV measurements (Fig. 2-12(C), (F), (I)), these three stainless steels were corroded more seriously. As for the Cr-rich stainless steel with a better corrosion resistance, there is no change on the surface morphology of before LSV (Fig. 2-12(J)) and after LSV measurements (Fig. 2-12(K), (L)). So no obvious corrosion occurred for the Cr-rich stainless steel. The possible reason is that the Cr-rich stainless steel contains highest content of the corrosion-resisting element Cr, the passive layer already existed on the surface of the Cr-rich stainless steel, and

so the polarization curve of the Cr-rich stainless steel has no active region.

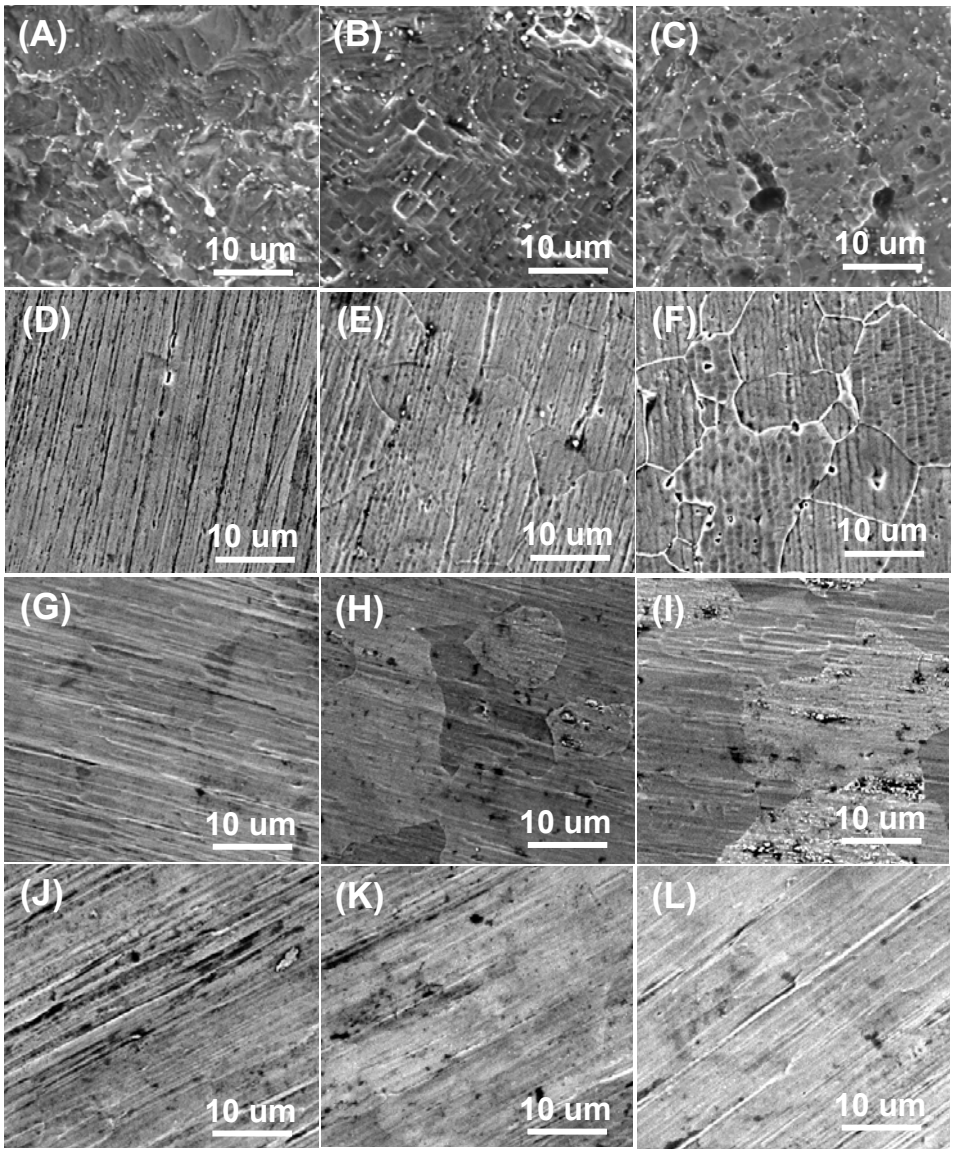

Fig. 2-12. SEM images of SUS410, SUS430, SUS445 and Cr-rich stainless steels before and after LSV measurements.

SUS410 (A) no LSV (B) LSV stopped at -0.02 V vs. SHE (C) LSV stopped at 1.1 V vs. SHE; SUS430 (D) no LSV (E) LSV stopped at -0.13 V vs. SHE (F) LSV stopped at 1.1 V vs. SHE; SUS450 (G) no LSV (H) LSV stopped at -0.22 V vs. SHE (I) LSV stopped at 1.1 V vs. SHE; Cr-rich (J) no LSV (K) LSV stopped at 0.26 V vs. SHE (L) LSV stopped at 1.1 V vs. SHE.

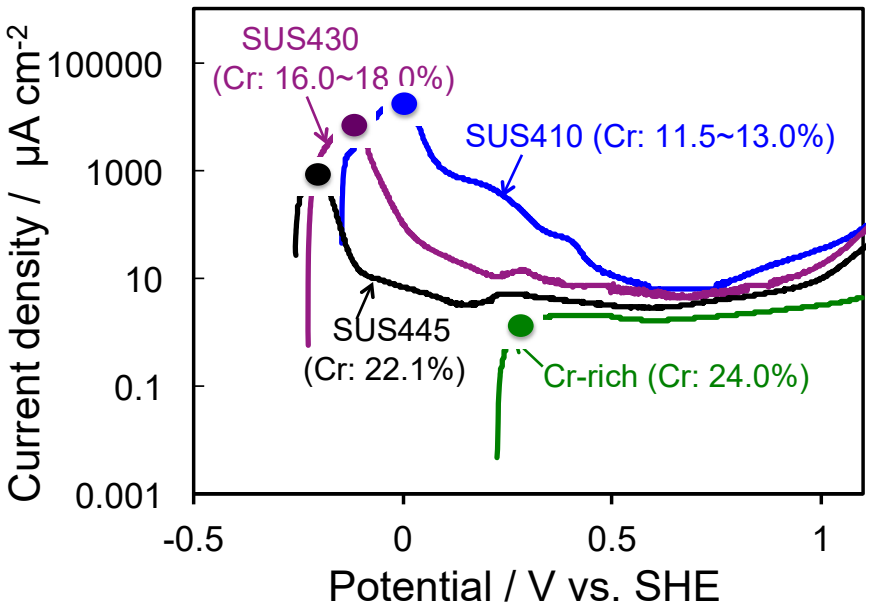

Fig. 2-13. The LSV measurement stopped position of the SUS410, SUS430, SUS445 and Cr-rich stainless steels.

2.3.5 Electrical conductivity

The electrical conductivities of the SUS410, SUS430, SUS445 and Cr-rich stainless steels were measured using a Mitsubishi Chemical "Loresta HP" (MCP-T410) electrometer by the four-point probe resistivity technique and the results are listed in Table 2-2. The volume resistivity of the four types of stainless steels decreased one order of magnitude compared to that of the graphite carbon. The 0.1 mm thick Cr-rich stainless steel with high corrosion resistance showed the same electrical conductivity as that of the 0.1 mm thick SUS445 stainless steel.

Table 2-2. Electrical conductivity of 4 types stainless steels and graphite carbon bipolar plate.

Sample name	Thickness (t / mm)	Surface Resistivity (Rs / Ω □$^{-1}$)	Volume Resistivity (Rs×t: R /Ω mm^{-1})
SUS410	3.9	2.97E-04	1.16E-03
SUS430	1	2.32E-03	2.32E-03
SUS445	0.1	3.17E-02	3.17E-03
Cr-rich	0.1	3.61E-02	3.61E-03
Graphite carbon (Bipolar plate of JARI standard cell)	18	6.29E-04	1.13E-02

2.4 Conclusions

In this study, the corrosion behavior of the four types ferritic stainless steels with different Cr contents have been experimentally investigated to study the effect of Cr content on the corrosion resistance of the ferritic stainless steels as bipolar plate of PEFC in sulfuric acid solution. The results showed that the ferritic stainless steel contains a higher Cr content, a better corrosion resistance is observed. Through the SEM images, no corrosion was happened for the Cr-rich stainless steel after LSV measurement from the rest potential to 0.26 V vs. SHE due to the highest Cr content. The conductivity of the Ni-free stainless steel did not decreased when increasing the Cr content.

References

[1] I. Rade, K. Koutzarov, E. Lefterova, G. Tsotridis, Influence of failure modes on PEFC stack and single cell performance and durability, . Int J Hydrogen Energy, 38 (2013), 7133-7139.

[2] X. Z. Yuan, H. Wang, J. Zhang and D. P. Wilkinson, Bipolar Plates for PEM Fuel Cells - From Materials to Processing, J. New. Mat. Electrochem. Systems., **8** (2005), 257-267.

[3] N. Baddoo and P. Francis, Development of design rules in the AISC design guide for structural stainless steel, Thin-Walled Struct., 83 (2014), 200-208.

[4] L. Gardner, The use of stainless steel in structure, Prog. Struct. Eng. Mater.,7(2) (2005), 45-55.

[5] F. Zhou and L. Li, Experimental study on hysteretic behavior of structural stainless steels under cyclic loading, J. Constr. Steel Res., 122 (2016), 94-109.

[6] X. Huang, D. Wang and Y. Yang, Effect of Precipitation on Intergranular Corrosion Resistance of 430 Ferritic Stainless Steel, J. Iron Steel Res. Int., 22(11) (2015), 1062-1068.

[7] S. Hastuty, A. Nishikata and T. Tsuru, Pitting corrosion of Type 430 stainless steel under chloride solution droplet, Corros. Sci., 52 (2010), 2035-2043.

[8] J. H. Sung, J. H. Kong, D. K. Yoo, H. Y. On, D. J. Lee and H. W. Lee, Phase changes of the AISI 430 ferritic stainless steels after high-temperature gas nitriding and tempering heat treatment, Mater. Sci. Eng. A, 489 (2008), 38-43.

[9] Y. Yu, S. Shironita, K. Nakatsuyama, K. Souma and M. Umeda, Surface composition effect of nitriding Ni-free stainless steel as bipolar plate of polymer electrolyte fuel cell, Appl. Surf. Sci., 388 (2016), 234-238.

[10] X. You, Z. Jiang and H. Li, Ultra-Pure Ferritic Stainless Steels-Grade Refining Operation and Application, J. Iron Steel Res. Int., 14(4) (2007), 24-30.

[11] D. Mercier, M. Bouttemy, J. Vigneron, P. Chapon, A. Etcheberry, GD-OES and XPS coupling: A new way for the chemical profiling of photovoltaic absorbers, Appl. Surf. Sci., 347 (2015), 799-807.

[12] T. Nelis, R. Payling, Glow Discharge Optical Emission Spectroscopy, Royal Society of Chemistry Cambridge, 2004.

[13] S. Suzuki, and K. Kakita, A Comparative Study of GDOES, SIMS and XPS Depth Profiling of Thin Layers on Metallic Materials, Journal of Surface Analysis, 12 (2) (2005), 174-177.

[14] D. Park, J. Yang, A. Vinu, A. Elzatahry and J. Choy, X-ray diffraction and X-ray absorption spectroscopic analyses for intercalative nanohybrids with low crystallinity, Arabian Journal of Chemistry, 9 (2016), 190-205.

[15] Y. Yu, S. Shironita, K. Nakatsuyama, K. Souma and M. Umeda, Influence of Nitriding Surface Treatment on Corrosion Characteristics of Ni-free SUS445 Stainless Steel, Electrochemistry, 84 (9) (2016), 709-713.

[16] JIS (Japanese Industrial Standards), (2007) G0579.

[17] J. C. Li, Y. Wang, D. C. Ba, Characterization of semiconductor surface

conductivity by using microscopic four-point probe technique, Physics Procedia, 32 (2012), 347-355.

[18] Y. Yu, S. Shironita, T. Mizukami, K. Nakatsuyama, K. Souma, M. Umeda, Corrosion-resistant characteristics of nitrided Ni-free stainless steel for bipolar plate of polymer electrolyte fuel cell, Int. J. Hydrogen Energy, 42 (2017), 6303-6309.

Chapter 3 Influence of nitriding surface treatment on corrosion characteristics of Ni-free SUS445 stainless steel

3.1 Introduction

Nowadays, the potential use of polymer electrolyte fuel cells (PEFCs) for residential applications and electric vehicles has been increasing the attention of researchers [1]. The practical operating voltage from one single cell cannot meet the requirements of such applications. Therefore, bipolar plates are used to connect the cells in series [2]. Bipolar plates are the important multifunctional components in the PEFC stacks with the significant functions of supplying reactant gases via flow channels, providing electrical connections between the individual cells and removing the produced water. In recent years, due to the high electrical conductivity, formability, manufacturability, gas impermeability and superior mechanical properties, metallic bipolar plates, such as stainless steel, have been widely studied by researchers [3,4,5]. However, there are still some issues not solved before the PEFC application can be commercialized. For example, the high cost and corrosion of the bipolar plates in the PEFC are significant problems that need to be studied in detail.

Generally, various stainless steels used as commercial bipolar plates are less chemically stable than competing PEFC electrode materials and the insufficient chemical stability of the bipolar plates will contaminate the electrolyte and degrade the energy efficiency of the cell [6]. However, many researchers have tried to improve

the corrosion resistance through diverse technologies, including the use of surface coatings, plasma-nitriding and gas-nitriding treatments [7,8,9]. Many different kinds of coatings, including carbon-based materials [10] and metal-based materials [11,12] have been introduced. However, the inherent defects of coatings, such as pinholes that can result in local corrosion and the high cost may hinder their application [13,14]. Nitriding treatment process is widely used over conventional gas to improve the surface hardness, mechanical properties, as well as corrosion resistance of stainless steels [15,16,17]. Yang Li [18] recently emphasized the nitrogen expanded austenite layer produced during high temperature plasma nitriding in a short time, reporting that high temperature plasma nitriding not only increased the surface hardness, but also improved the corrosion resistance of the austenitic stainless steel and the nitrided layer was shown to consist of expanded austenite γ_N and small amounts of free-CrN and iron nitrides.

Without the expensive nickel element, the SUS445 stainless steel [19] can lower the cost of the PEFCs. The purpose of this present study is to improve the corrosion resistance of the Ni-free SUS445 stainless steel using a nitriding heat treatment technology. The influence of the nitriding process on the microstructure, morphology, surface element component and corrosion behavior in a 0.5 mol dm^{-3} H_2SO_4 solution of Ni-free SUS445 stainless steel was investigated.

3.2 Experimental

3.2.1 Material and heat treatment

The sample used in this study was Ni-free SUS445 stainless steel made by Nisshin Steel Co., Ltd., Japan. The chemical compositions (mass%) of the SUS445 and SUS316 stainless steels are shown in Table 3-1. Compared to the SUS316 stainless steel, there is no nickel component in the SUS445 stainless steel, while small amounts of Al, Ti, and Nb elements are present.

Table 3-1. Chemical components of SUS445 and SUS316 stainless steels (mass%).

	Fe	Al	Ni	Cr	Mo	Mn	Si	Ti	Nb	C
SUS445	Bal.	0.09	-	22.1	1.20	0.20	0.18	0.19	0.23	0.01
SUS316	Bal.	-	10.0~14.0	16.0~18.0	2.0~3.0	≤2.0	≤1.0	-	-	≤0.08

From Nisshin Steel Co., Ltd.

The surface heat treatments were carried out in a vacuum furnace. The SUS445 stainless steels were cut in small pieces and cleaned before nitriding. The nitriding heat treatments were performed at 1473 K (SUS445-N1) and 1373 K (SUS445-N2) under a nitrogen (purity: 99.995%) atmosphere. The SUS445-Ar stainless steel was heat-treated SUS445 stainless steel under an argon (purity: 99.995%) atmosphere at 1423 K. Two different heat treatment atmospheres were used for studying the effect of the nitriding heat treatments on the characteristics of the SUS445 stainless steel. The

heat treatment conditions and schematic images of nitriding treatment procedure of SUS445 stainless steel are shown in Table 3-2.

Table 3-2. Heat treatment conditions and schematic images of nitriding treatment procedure of SUS445 stainless steel.

Sample name	Heating temperature / K	Atmosphere
SUS445	-	-
SUS445-N1	1473	N_2 gas
SUS445-N2	1373	N_2 gas
SUS445-Ar	1423	Ar gas

SUS445-N1 (SUS445-N in chapter 4)

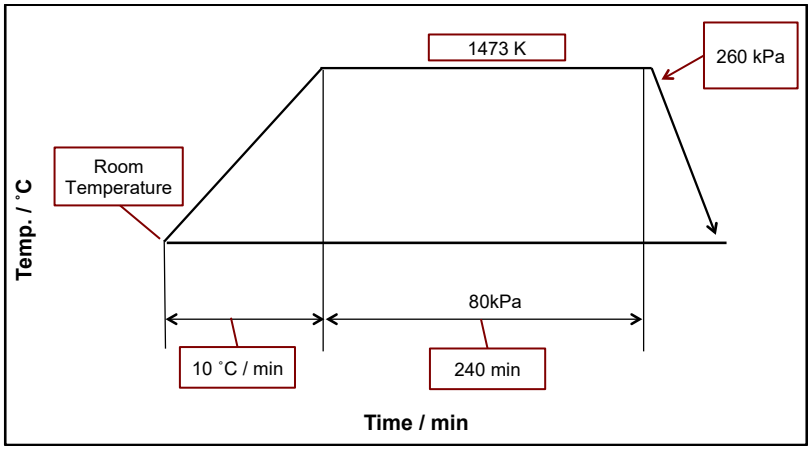

SUS445-N2

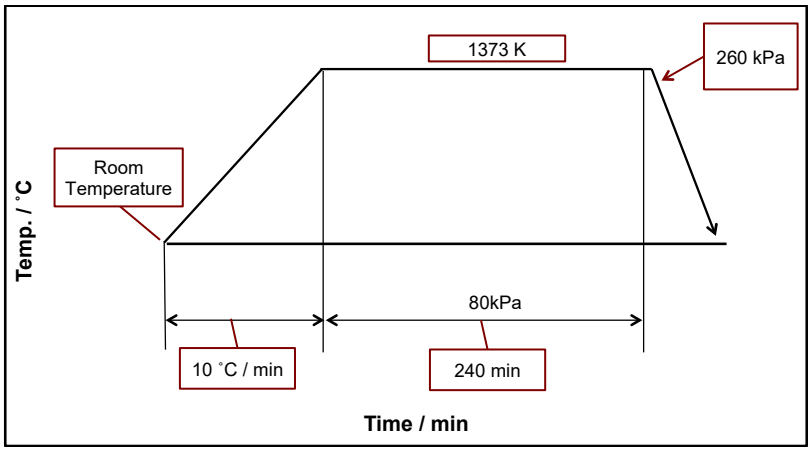

3.2.2 Characterizations

For the structural characterization, X-ray diffraction (XRD) measurements were performed using an XRD-6100 (Shimadzu) instrument in the θ-2θ geometry with Cu Kα radiation (λ = 1.5406 Å) generated at 40 kV and 30 mA; 2θ was scanned from 10° to 110° at the scan rate of 2° min^{-1}. The surface compositions of the heat-treated stainless steels were measured by glow discharge optical emission spectroscopy (GD-OES, Horiba GD-Profiler 2). GD-OES is a rapid depth profiling technique that we can obtain the profile of atomic percent vs. time [20]. The surface of the sample was sputtered by argon ions and the argon pressure was 400 Pa. The analyzed spot size was 4 mm in diameter. The mainly investigated elements on the surface of the heat-treated samples were Fe, C, N, Cr, Al, etc.

The electrochemical technique used in this study was linear sweep voltammetry (LSV). The electrochemical measurements were conducted using an ALS/[H] CH Instruments Electrochemical Analyzer Model 802B with a three-electrode cell at room temperature. A schematic image of the electrochemical three-electrode cell is shown in Fig. 3-1. A platinum coil was used as the counter electrode, Ag/Ag_2SO_4 [21,22] was used as the reference electrode and the working electrode was the heat-treated stainless steel specimen. All the potentials used in this study were converted to the standard hydrogen electrode (SHE) after the LSV measurements. The electrolyte was a 0.5 mol dm^{-3} H_2SO_4 solution. Before the LSV measurement, the stainless steels were washed with acetone and distilled water for 5 min during sonication, then a 30-min Ar gas bubbling was conducted. Subsequently, the cathodic

treatment was carried out at the potential of -0.47 V vs. SHE for 1 min and maintained in the cell under the rest potential for 5 min. During this step, the invisible H_2 gas generated on the surface of the sample was removed by Ar bubbling. For the electrochemical measurement, the scan potential was in the range of the rest potential to 1.1 V vs. SHE and the scan rate was 0.33 mV s^{-1} [23]. The surface morphologies and cross sectional images of the samples were observed by scanning electron microscopy (SEM, JSM-6060A, JEOL Ltd.). Energy-dispersive X-ray spectroscopy (EDX) was performed using the SEM system to obtain the chemical composition of the surface.

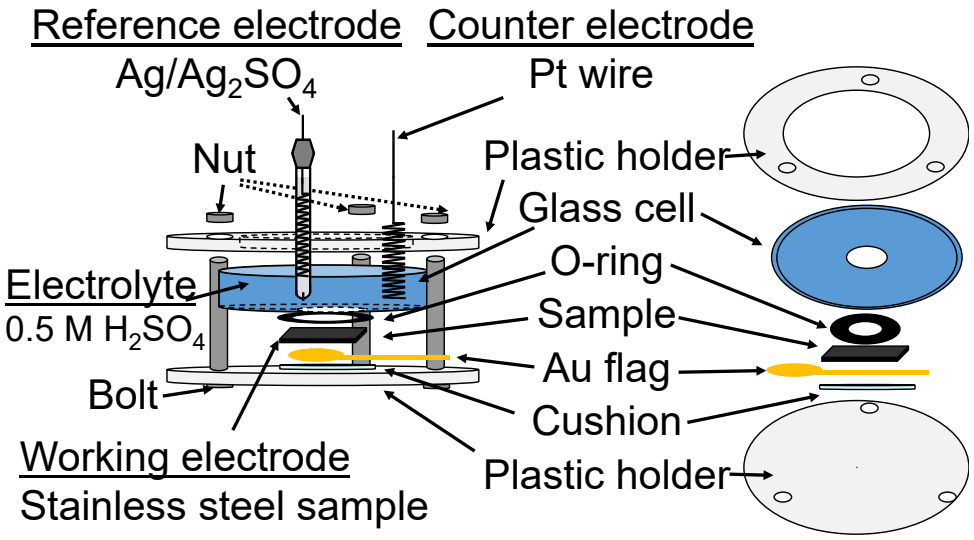

Fig. 3-1. The schematic image of electrochemical three-electrode cell.

3.3 Results and discussion

3.3.1 X-ray diffraction analysis

Figure 3-2 shows the XRD patterns of the SUS445, SUS445-N1, SUS445-N2, and SUS445-Ar stainless steels. In the case of the untreated SUS445 stainless steel and SUS445-Ar stainless steel heat-treated under the argon atmosphere, the diffraction spectra show α-Fe (body centered cubic: BCC) peaks. However, for the SUS445-N1 stainless steel heat-treated under the nitrogen atmosphere at 1473 K, the γ-Fe (face centered cubic: FCC) was transformed from α-Fe by a solid solution effect of the nitrogen [24], and "expanded austenite" γ_N(111) and AlN phases formed. The γ_N(111) phase appeared at lower angles than the γ(111) peak, suggesting a higher lattice parameter than the substrate austenite due to the dissolution of the nitrogen atoms [25].With a lower nitriding temperature, the diffusion and solid solution of N became slowly and part of the α-Fe was transformed into the γ-Fe phase for the SUS445-N2 stainless steel heat-treated under the nitrogen atmosphere at 1373 K; both the α-Fe and γ-Fe phases existed. The XRD patterns of the SUS445-N2 stainless steel also consist of γ_N(111) and AlN phases, and new phases of CrN and Cr_2N were detected. The amount and crystal size of formed Cr-N phase for the SUS445-N1 stainless steel was so small that it is very difficult to be detected by XRD measurement. In this study, because the SUS445 stainless steel includes the element Al, after the nitriding heat treatment, the AlN phase was detected.

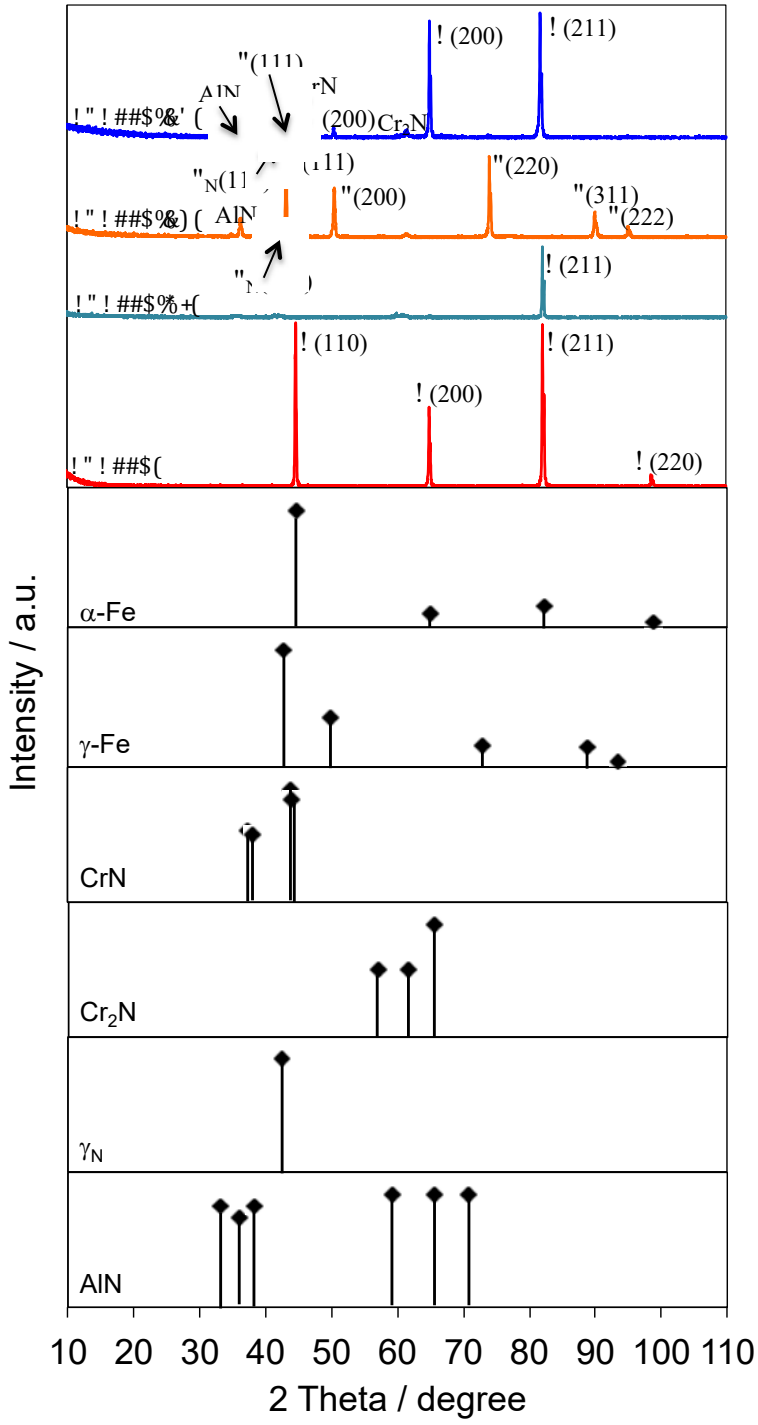

Fig. 3-2. XRD patterns of SUS445, SUS445-N1, SUS445-N2 and SUS445-Ar stainless steels.

3.3.2 GD-OES analysis

The depth profile measurement results for the SUS445, SUS445-N2 and SUS445-Ar specimens using GD-OES are shown in Fig. 3-3. Based on the GD-OES results, the peaks of the N and Al elements appeared on the surface of the heat-treated SUS445-N2 and SUS445-Ar stainless steels. However, the Cr content on the surface of the SUS445-Ar stainless steel was significantly reduced compared to that of the SUS445 stainless steel and no Cr-N compounds were detected according to the XRD results. Due to that the Ar atmosphere contained a small amount of N_2, according to the Cr-N phase diagram [26], at low pressure, even a small amount of N_2 has the tendency to form Cr-N and diffuse into the stainless steel, so the N content showed peak for the SUS445-Ar stainless steel. For the nitrided stainless steels, the N content of the SUS445-N1 stainless steel was 38.5%, which was not very different with that of the SUS445-N2 stainless steel.

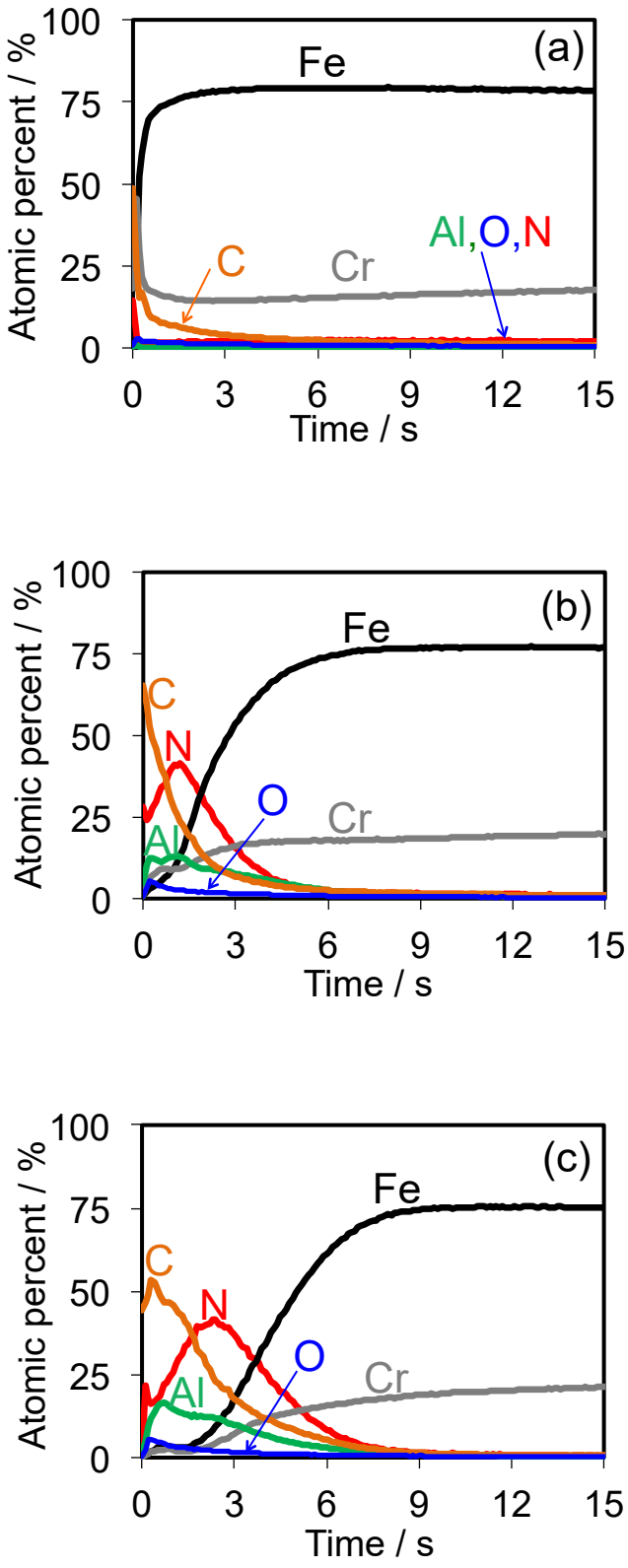

Fig. 3-3. GD-OES results of SUS445, SUS445-N2 and SUS445-Ar stainless steels.

(a) SUS445; (b) SUS445-N2; (c) SUS445-Ar.

3.3.3 Cross-sectional observation

Figure 3-4 shows the cross-sectional SEM images of the SUS445 and SUS445-N2 stainless steels along with the EDX results. The nitride layer of SUS445-N2 stainless steel is at least 1 μm according to the SEM image. At the surface of the SUS445-N2 stainless steel after a nitriding treatment at 1373 K, some dot and linear substances precipitated. Based on an analysis of the chemical compositions of points 1, 2 and 3 on the surface of the SUS445-N2 stainless steel by an EDX measurement, the results revealed that the substrate region 1 contained the Cr-N phase. For the dot precipitation 2, the Al and O contents had increased significantly compared to the substrate region, while other elements had decreased in content, suggesting that the dot precipitation 2 was the Al-O phase. Compared to point 1, the Al and N contents in the precipitation 3 had increased, while the other compositions decreased, indicating that the linear precipitation 3 was the Al-N compound. The EDX results show that the Cr-N, Al-O and Al-N compounds exist on the surface of the nitrided SUS445-N2 stainless steel.

At nitriding temperature 1373 K, the Al, N and O contents were rearranged on the surface of the SUS445-N2 stainless steel, the Al element diffused from the inside of the stainless steel to its surface. So the Al, N and O elements had high contents on the surface of the SUS445-N2 stainless steel, and the Al-N and Al-O phases were easily formed. The aluminum nitride and chromium nitride is semiconductor [27, 28] and aluminum oxide is an electrical insulator [29].

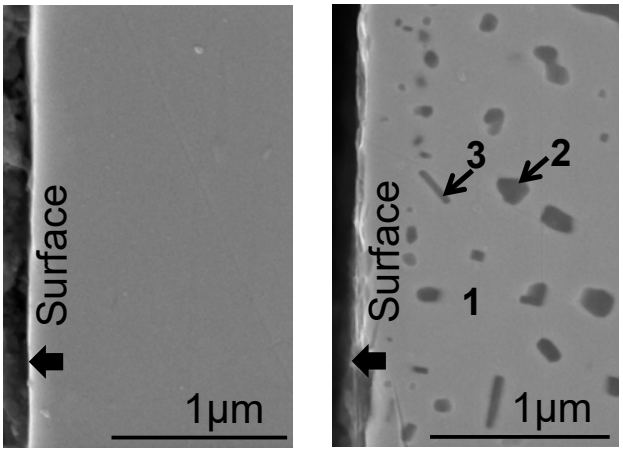

EDX results of point 1, 2 and 3 (at. %)

	1 base	2 dot	3 line
N	8.9	5.6	39.9
O	13.2	31.3	1.5
Al	0.3	22.8	45.0
Cr	18.0	10.1	3.7
Fe	58.5	29.7	9.5

Fig. 3-4. Cross-sectional SEM images and EDX results of SUS445 and SUS445-N2 stainless steels.

3.3.4 Corrosion behavior

The potentiodynamic polarization curves of the untreated and heat-treated samples in the Ar-saturated 0.5 mol dm^{-3} H_2SO_4 electrolyte at room temperature are shown in Fig. 3-5. Although there is no nickel content in the SUS445 stainless steel, the current densities in the passive region of the SUS445 stainless steel are almost the same as those of the SUS316 stainless steel. For the untreated and heat-treated SUS445 stainless steels, the onset potentials nearly have no big difference. In the case of the heat-treated SUS445-Ar stainless steel under an Ar atmosphere, the current densities in the active and passive regions are the highest among all the samples, thus showing a poor corrosion resistance. The polarization curves of the nitrided SUS445-N1 and SUS445-N2 stainless steels exhibit lower current densities than the untreated SUS445 stainless steel in the both active and passive regions, especially for the SUS445-N2

stainless steel. This means that the corrosion resistance of the SUS445 stainless steel is improved after the nitriding heat treatment [30,31]. The benefits of the γ_N, Al-N and Cr-N phases to the corrosion resistance have been found by many researchers [32,33,34]. Due to the presence of the γ_N, AlN, CrN and Cr_2N phases, the corrosion resistance of the SUS445-N2 stainless steel is the best. After the LSV measurement, the ratio of N to Cr of the SUS445-N2 stainless steel almost no changed compared with that of the SUS445-N2 stainless steel before LSV measurement.

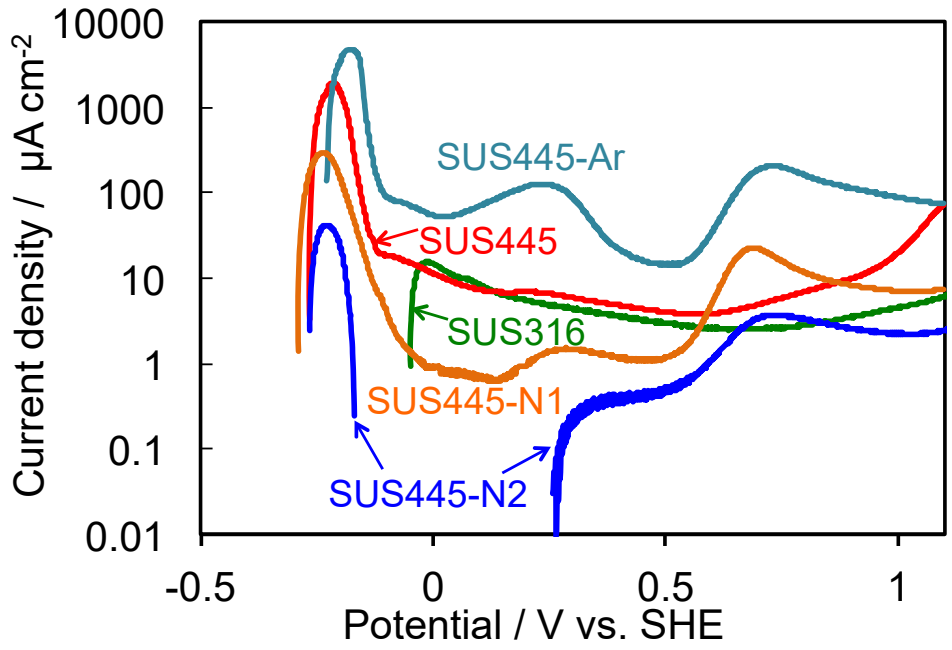

Fig. 3-5. Polarization curves of untreated (SUS445 and SUS316) and heat-treated stainless steels (SUS445-N1, SUS445-N2 and SUS445-Ar) in Ar-saturated 0.5 mol dm^{-3} H_2SO_4 electrolyte at room temperature.

3.3.5 Surface morphology analysis

Figure 3-6 is SEM images of the SUS445, SUS445-N1, SUS445-N2 and SUS445-Ar stainless steels measured at a magnification of 2000 × before and after the LSV measurements. Based on the SEM images, after the LSV measurement, the surface of the SUS445 stainless steel was corroded and the grain boundaries became visible. Because the boundaries of the SUS445 stainless steels are more susceptible to corrosion than their insides, an intergranular corrosion occurred in the SUS445 stainless steel. For the SUS445-Ar stainless steel, a more significant corrosion occurred after the LSV measurement, where the grain boundary can be more clearly seen and became separated due to chemical attack by the acid solution. The type of corrosion of the SUS445-Ar stainless steel was also intergranular corrosion. Comparing the SEM images of the SUS445-N1 stainless steel after the LSV to before the LSV, there was no observed grain boundary while only the number of pitting holes increased. This means that a slight pitting corrosion occurred for the SUS445-N1 stainless steel. The corrosion damage of the SUS445-N1 stainless steel was greatly less than the untreated SUS445 and SUS445-Ar stainless steels. As for the SUS445-N2 stainless steel, less pitting holes were found than the SUS445-N1 stainless steel after the LSV measurement resulting in the lower passive current densities. Due to that the SUS445-N1 stainless steel has numbers of pitting holes after the LSV measurement, the surface morphology of the SUS445-N1 and SUS445-Ar stainless steels was compared.

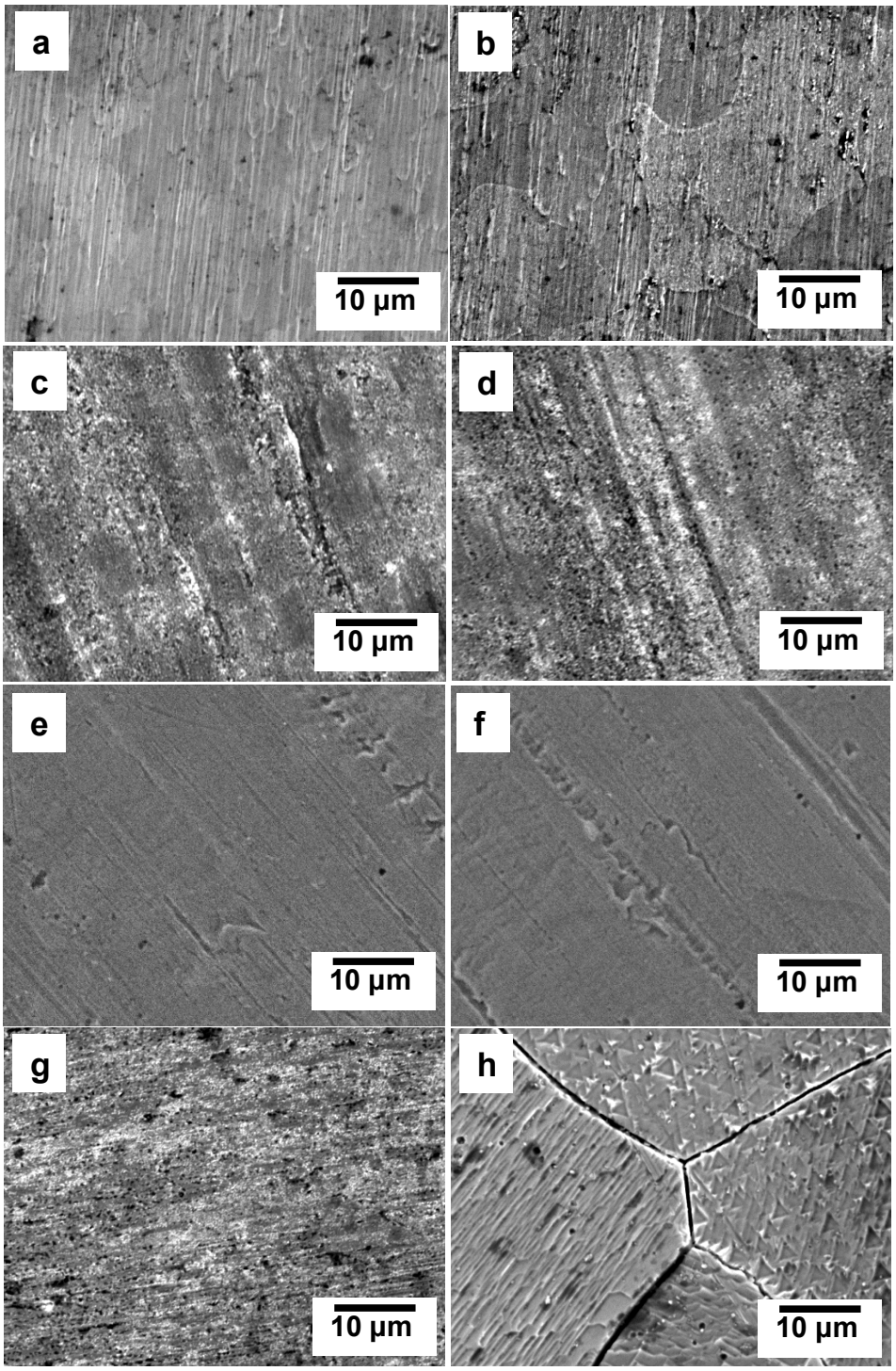

Fig. 3-6. SEM images of SUS445, SUS445-N1, SUS445-N2 and SUS445-Ar stainless steels at magnification of 2000 × before and after LSV measurements.

SUS445 (a) before LSV (b) after LSV; SUS445-N1 (c) before LSV (d) after LSV; SUS445-N2 (e) before LSV (f) after LSV; SUS445-Ar (g) before LSV (h) after LSV.

Figure 3-7 shows SEM images of the SUS445-N1 and SUS445-Ar stainless steels at the higher magnification of 5000 × after the LSV measurements. From the SEM images, it can be seen that the grain morphology of the SUS445-Ar stainless steel was totally different from that of the SUS445-N1 stainless steel and corroded more significantly than the SUS445-N1 stainless steel.

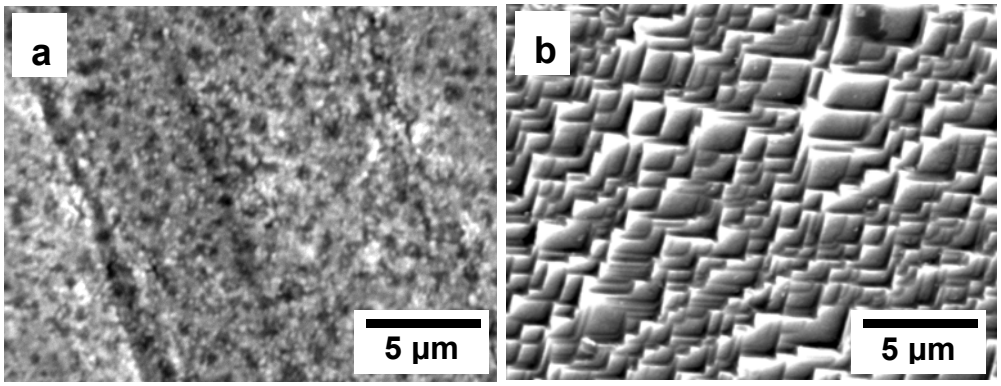

Fig. 3-7. SEM images of SUS445-N1 and SUS445-Ar stainless steels at magnification of 5000 × after LSV measurements.

(a) SUS445-N1; (b) SUS445-Ar.

Figure 3-8 shows surface schematic images of nitrided SUS445-N stainless steel and SUS445-Ar stainless steel heat-treated under Ar atmosphere. After nitriding heat treatment, the Al and N elements on the surface of the nitrided sample increased and formed new phases (Cr-N, Al-N and γ_N) that are beneficial for the corrosion resistance, so the polarization current densities in the active and passive regions of the nitrided sample are lowest among all the samples. After LSV measurement, the surface of the nitrided sample was corroded slightly and no grain was corroded.

However, the corrosion resistance of the SUS445-Ar sample was decreased due to the lack of Cr content on its surface, after LSV measurement, the surface of the SUS445-Ar sample was corroded seriously and the grain was also corroded.

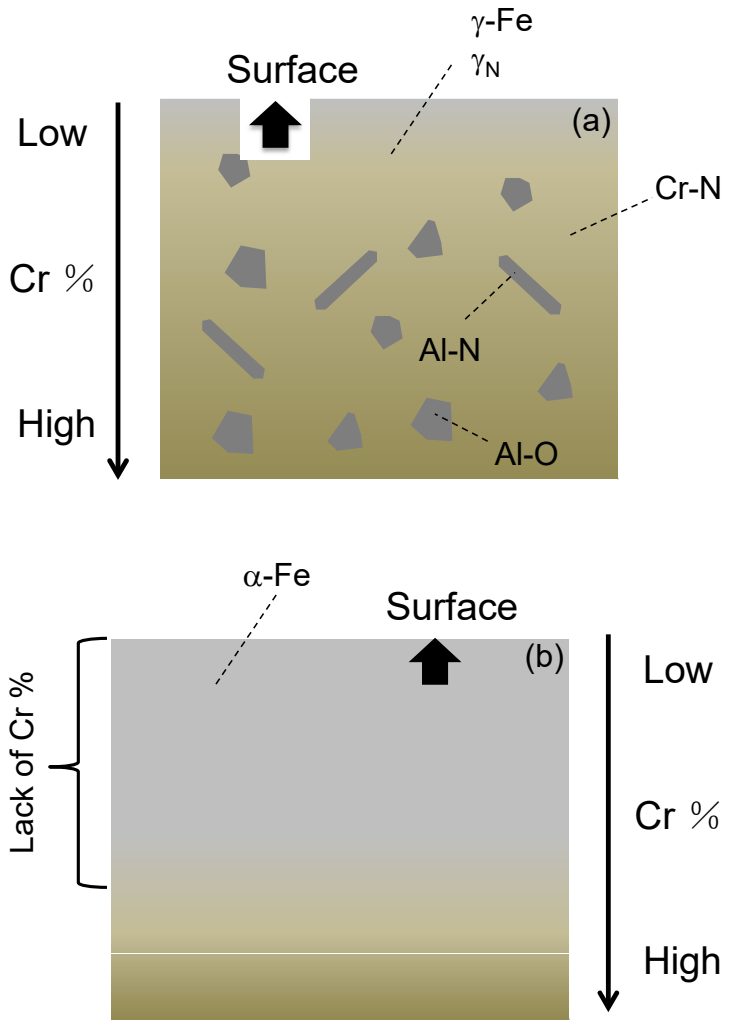

Fig. 3-8. Surface schematic images of (a) nitrided SUS445-N stainless steel and (b) SUS445-Ar stainless steel heat-treated under Ar atmosphere.

3.3.6 Discussion

As an effective route to improve the corrosion resistance of the Ni-free SUS445 stainless steel in the H_2SO_4 solution, the nitriding treatment process was investigated in this study. The strong affinity between nitrogen and Cr enabled the permeation of nitrogen from the surface of the stainless steel into the interior. The structure and composition in the surface layer of the nitrided stainless steel changed and the corrosion resistance was increased because of the formation of new phases. However, the relationship between the nitriding parameters and characteristics of the stainless steel need to be further investigated. Future study for the nitrided SUS445 stainless steel will focus on the modification of the nitriding parameters to achieve a better corrosion resistance. Therefore, the nitrided SUS445 stainless steel can be applied in a wide filed.

3.4 Conclusions

In this study, Ni-free SUS445 stainless steels were heat treated under a nitrogen atmosphere at 1473 K and 1373 K, and heat treatment was also performed under an argon atmosphere at 1423 K for comparison. After the nitriding heat treatment, the γ-Fe phase was transformed from α-Fe. The AlN, γ_N(111), CrN and Cr_2N phases also formed on the surface of the nitrided SUS445-N1 stainless steel heat treated at 1373 K. However, only the AlN and γ_N(111) phases were detected in the SUS445-N2 stainless steel heat treated at 1473 K.

All the nitrided samples showed a better corrosion resistance in the Ar-saturated 0.5 mol dm^{-3} H_2SO_4 solution compared to the untreated and heat-treated samples under an argon atmosphere. The corrosion type of nitrided sample was pitting corrosion different from the untreated and heat-treated samples under an argon atmosphere, which was intergranular corrosion.

Reference

[1] X. Z. Yuan, H. Wang, J. Zhang, D. P. Wilkinson, Bipolar plates for PEM fuel cells-from materials to processing, J. New Mater. Electrochem. Syst., 8 (2005), 257-267.

[2] S. Karimi, N. Fraser, B. Roberts, F. R. Foulkes, A review of metallic bipolar plates for proton exchange membrane fuel cells: materials and fabrication methods, Adv. Mater. Sci. Eng., 2012 (2012), 1-22.

[3] J. Lv, T. Liang, W. Guo, Effect of strain on corrosion resistance of 316L stainless steel as bipolar plates in PEMFC environment. Int. J. Hydrogen Energy, 40 (2015), 10382-10389.

[4] R. A. Antunes, M. C. L. Oliveira, G. Ett, V. Ett. Corrosion of metal bipolar plates for PEM fuel cells: a review, Int. J. Hydrogen Energy, 35 (2010), 3632-3647.

[5] K. H. Lee, S. H. Lee, J. H. Kim, Y. Y. Lee, Y. H. Kim, M. C. Kim, D. M. Wee, Effects of thermal oxi-nitridation on the corrosion resistance and electrical conductivity of 446M stainless steel for PEMFC bipolar plates, Int. J. Hydrogen Energy, 34 (2009), 1515-1521.

[6] Y. S. Jeong, Y. T. Jeon, H. G. Seong, S. G. Lim, Electrochemical characteristics of 316L stainless steel processed with a thermally treated Ni- and Cr-rich surface coating, Met. Mater. Int., 15 (2009), 37-42.

[7] A. S. Woodman, E. B. Anderson, K. D. Jayne, M. C. Kimble, Development of corrosion-resistant coatings for fuel cell bipolar plates, AESF SUR/FIN '99

Proceedings, (1999), 717-725.

[8] S. Sato, Y. Arai, N. Yamashita, A. Kojyo, K. Kodama, N. Ohtsu, Y. Okamoto, K. Wagatsuma, Surface-nitriding treatment of steels using microwave-induced nitrogen plasma at atmospheric pressure, Appl. Surf. Sci., 258 (2012), 7574-7580.

[9] D. Q. Peng, T. H. Kim, J. H. Chung, J. K. Park, Development of nitride-layer of AISI 304 austenitic stainless steel during high-temperature ammonia gas-nitriding, Appl. Surf. Sci., 256 (2010), 7522-7529.

[10] Y. J. Ren, J. Chen, C. L. Zeng, Corrosion protection of type 304 stainless steel bipolar plates of proton-exchange membrane fuel cells by doped polyaniline coating, J Power Sources, 195 (2010), 1914-1919.

[11] R. Tian, J. Sun, Corrosion resistance and interfacial contact resistance of TiN coated 316L bipolar plates for proton exchange membrane fuel cell, Int. J. Hydrogen Energy, 36 (2011), 6788-6794.

[12] Y. H. Yun, Deposition of gold-titanium and gold-nickel coatings on electropolished 316L stainless steel bipolar plates for proton exchange membrane fuel cells, Int. J. Hydrogen Energy, 35 (2010), 1713-1718.

[13] K. Lin, X. Li, Y. Sun, X. Luo, H. Dong, Active screen plasma nitriding of 316 stainless steel for the application of bipolar plates in proton exchange membrane fuel cells, Int. J. Hydrogen Energy, 39 (2014), 21470-21479.

[14] R. Tian, J. Sun, J. Wang, Study on behavior of plasma nitrided 316L in PEMFC working conditions, Int. J. Hydrogen Energy, 33 (2008), 7507-7512.

[15] L. Wang, S. Ji, J. Sun, Effect of nitriding time on the nitrided layer of AISI 304 austenitic stainless steel, Surf. Coat. Technol., 200 (2006), 5067-5070.

[16] J. H. Sung, J. H. Kong, D. K. Yoo, H. Y. On, D. J. Lee, H. W. Lee, Phase changes of the AISI 430 ferritic stainless steels after high-temperature gas nitriding and tempering heat treatment, Mater. Sci. Eng., A 489 (2008), 38-43.

[17] C. V. Franco, F. G. Mittelstadt, J. L. R. Muzart, A. R. Souza, L. P. Cardoso, Plasma surface treatment of AISI 4140 steel for improved corrosion resistance, J. Mater. Sci., 31 (1995), 431-435.

[18] Y. Li, Z. Wang, L. Wang, Surface properties of nitrided layer on AISI 316L austenitic stainless steel produced by high temperature plasma nitriding in short time, Mater. Lett., 128 (2014), 231-234.

[19] K. Miura, K. Nakatsuyama, M. Umeda, Development of fuel cell separators using nitrogen containing stainless steel, Electrochemistry, 80 (2012), 1012-1016.

[20] A. Thobor, C. Rousselot and S. Mikhailov, Depth profiles study of n(TiN+AlN) bilayers systems by GDOES and RBS techniques, Surf. Coat. Tech., 351 (2003), 174-175.

[21] M. Umeda, Y. Kuwahara, A. Nakazawa and M. Inoue, Pt degradation mechanism in concentrated sulfuric acid studied using rotating ring−disk electrode and electrochemical quartz crystal microbalance, J. Phys. Chem. C., 113 (2009), 15707.

[22] D. J. G. Ives and G. J. Janz, Reference electrodes, theory and practice, Academic Press, New York and London, Chap. 8 (1961).

[23] Y. Yu, S. Shironita, K. Nakatsuyama, K. Souma and M. Umeda, Influence of Nitriding Surface Treatment on Corrosion Characteristics of Ni-free SUS445 Stainless Steel, Electrochemistry, 84 (9) (2016), 709-713.

[24] S. Sato, Y. Arai, N. Yamashita, A. kojyo, K. kodama, N. Ohtsu, Y. Okamoto and K. Wagatsuma, Surface-nitriding treatment of steels using microwave-induced nitrogen plasma at atmospheric pressure, Appl. Surf. Sci., 258 (2012), 7574.

[25] L. H. Lin, S. C. Chen, C. Z. Wu, J. M. Hung and K. L. Ou, Microstructure and antibacterial properties of microwave plasma nitrided layers on biomedical stainless steels, Appl. Surf. Sci., 257 (2011), 7375.

[26] B. Predel, Cr-N (Chromium-Nitrogen), Landolt-Börnstein-Group IV Physical Chemistry, Vol. 5d, Springer Berlin Heidelberg, (1994), 1-3.

[27] L. I. Berger. Semiconductor Materials. CRC Press. ISBN 0-8493-8912-7. Retrieved 20140101, (1997), 123-124.

[28] I. Batko, M. Batkova, F. Lofaj, Electrical resistivity of CrN thin films, Acta Physica Polonica A, 125 (2014), 415-416.

[29] Material Properties Data: Alumina (Aluminum Oxide). Makeitfrom.com. Retrieved on 20130417.

[30] Y. Yu, S. Shironita, K. Nakatsuyama, K. Souma and M. Umeda, Surface composition effect of nitriding Ni-free stainless steel as bipolar plate of polymer electrolyte fuel cell, Appl. Surf. Sci., 388 (2016), 234-238.

[31] Y. Yu, S. Shironita, T. Mizukami, K. Nakatsuyama, K. Souma, M. Umeda,

Corrosion-resistant characteristics of nitrided Ni-free stainless steel for bipolar plate of polymer electrolyte fuel cell, Int. J. Hydrogen Energy, 42 (2017), 6303-6309.

[32] Y. Li, Z. Wang and L. Wang, Low temperature anodic nitriding of AISI 304 austenitic stainless steel, Mater. Lett., 128 (2014), 231.

[33] F. Haftlang, A. Habibolahzadeh and M. H. Sohi, Improving electrochemical properties of AISI 1045 steels by duplex surface treatment of plasma nitriding and aluminizing, Appl. Surf. Sci., 329 (2015), 240.

[34] A. Ruden, E. Restrepo-Parra, A. U. Paladines and F. Sequeda, Corrosion resistance of CrN thin films produced by dc magnetron sputtering, Appl. Surf. Sci., 270 (2013), 150.

Chapter 4 Corrosion-resistant characteristics of nitrided Ni-free stainless steel for bipolar plate of polymer electrolyte fuel cell

4.1 Introduction

As a strong contender, the polymer electrolyte fuel cell (PEFC) that converts the chemical energy of the reactant into electrical energy is one of the most promising clean energy converters in the coming years [1-5]. The polymer electrolyte fuel cell has received significant attention for use in fuel cell vehicles and stationary applications due to its high power density, low operating temperature and pressure, quick startup, low noise emissions and high-energy conversion efficiency compared to traditional power sources [6-12]. Some automobile companies have already installed a PEFC in a fuel cell vehicle. The bipolar plate is a key component of the PEFC with several essential functions, including connecting individual cells in the stacks, providing pathways for the reactant gases, carrying current away from the cell and providing structure support for the entire stack [13-15]. Two types of bipolar plates, metallic- and carbon-based, are commercially available [16]. Carbon-based bipolar plates, particularly graphite, are popular for the PEFC [17, 18]. However, the disadvantages of poor mechanical properties and brittleness during fabrication lead to the high cost of the graphite bipolar plate [19].

The metallic bipolar plates are thinner than the graphite bipolar plates resulting in a light weight, low volume and decreased cost for the PEFC [20-22]. As an alternative

material for bipolar plates, metallic bipolar plates usually have a corrosion problem that can degrade the output power of the PEFC.

Conventional surface coating methods used to improve the corrosion resistance of materials typically leave inherent defects, such as pinholes, that result in accelerated local corrosion and limit their application [23]. Therefore, a nitriding process is introduced as a widely employed thermochemical surface treatment to improve the corrosion resistance, fatigue and wear resistance of the stainless steel and alloys [24].

In this study, in order to reduce the use of nickel and decrease the cost of the PEFC, we report a study of the nitriding treatment of Ni-free SUS445 stainless steel [25] without an expensive nickel content and with an extra high content of the corrosion-resisting element, Cr (22.1%), at a high temperature (>1000°C). The aims of this study are to prepare the anti-corrosion Ni-free SUS445 stainless steel by a nitriding treatment used for one component of the PEFC, i.e., the bipolar plate, and investigate its mechanism. The corrosion behavior and electrical resistivity of the nitrided surface layer were evaluated based on the Japanese Industrial Standards [26] and by the four-point probe method [27].

4.2 Experimental procedure

4.2.1 Material and specimen preparation

The Ni-free SUS445 stainless steel made by Nisshin Steel Co., Ltd., Japan, was used for the surface treatment. Compared to the SUS430 and SUS410 stainless steels, the high content of Cr and added molybdenum give it some significant technical benefits. The chemical components of the SUS445, SUS430 and SUS410 stainless steels are shown in Table 4-1.

Table 4-1. Chemical components of SUS445, SUS430 and SUS410 stainless steels (mass%).

	Fe	Al	Ni	Cr	Mo	Mn	Si	Ti	Nb	C
SUS445[a]	Bal.	0.09	-	22.1	1.20	0.20	0.18	0.19	0.23	0.01
SUS430[b]	Bal.	-	-	16.0~18.0	-	≤1.0	≤0.75	-	-	≤0.12
SUS410[b]	Bal.	-	-	11.5~13.0	-	≤1.0	≤0.50	-	-	≤0.15

[a]From Nisshin Steel Co., Ltd.

[b]From The Nilaco Corporation Co., Ltd.

Before the nitriding surface treatment, the 1.5-mm thick SUS445 stainless steel plate was cut into pieces with the dimensions of 10 mm × 15 mm and cleaned with ethanol. The nitriding treatment was carried out in a vacuum furnace at 1200°C for 4h under a nitrogen atmosphere (SUS445-N). A Cr-N coated SUS445 specimen was prepared by an ion plating technique (Cr-N/SUS445) in order to study the influence of

the Cr-N phase on the corrosion resistance of the SUS445 stainless steel. The schematic image and equipment of ion plating technique is shown in Fig. 4-1. SUS445 stainless steel was the substrate material, the target was Cr and the atmosphere used was nitrogen gas. The flow rate of the N_2 during the ion plating experiment was 410 cm^3 min^{-1} and the arc current was 200-250 A.

The surface treatment conditions of the SUS445 stainless steel are shown in Table 4-2.

IPB-450, Nakatsuyama Heat Treatment Co., Ltd.

(a) Schematic image (b) Equipment

Fig. 4-1. Schematic image and equipment of ion plating technique.

Table 4-2. Surface treatment conditions of the SUS445 stainless steel.

Sample	SUS445-N	Cr-N/SUS445
Surface treatment	Nitriding	Ion plating
Gas	N_2	N_2: 410 mL min^{-1}
Other parameter	Temperature: 1200°C	Arc current: 200-250 A

4.2.2 Electrochemical test

The corrosion resistance of the untreated and treated stainless steel was evaluated by a linear sweep voltammetry (LSV) measurement conducted by an ALS/[H] CH Instruments Electrochemical Analyzer Model 802 B. The polarization curve was measured based on the Japanese Industrial Standards [26]. A platinum coil was used as the counter electrode, Ag/Ag_2SO_4 was used as the reference electrode and the working electrode was the stainless steel specimen. The electrolyte was a 0.5 mol dm^{-3} H_2SO_4 solution. All the potentials used in this study were converted to the standard hydrogen electrode (SHE) after the LSV measurements. For the electrochemical measurement, the scan potential was from the rest potential to 1.1 V vs. SHE after the -0.47 V vs. SHE polarization for 1 min. The scan rate was 0.33 mV s^{-1}.

4.2.3 Surface layer analysis

The scanning electron microscopy (SEM) technique (JSM-6060A, JEOL Ltd.) was used to observe the microstructure and morphology of the untreated and nitrided samples before and after the LSV measurements. The phases present in the surface layer were identified by an X-ray diffraction analysis (XRD-6100, Shimadzu) with Cu Kα radiation (λ = 1.5406 Å) generated at 40 kV and 30 mA in the 2θ range from 10° to 80°. The change in the element content from the surface to the interior of the nitrided sample was analyzed by glow discharge optical emission spectroscopy (GD-OES, Horiba GD-Profiler 2). In order to determine the surface chemical

characterization after the nitriding treatment, an X-ray photoelectron spectroscopy (XPS) measurement was performed using an X-ray source. The sample was sputtered by argon ions to different depths.

4.3 Results and discussion

4.3.1 Polarization curve

The polarization curves of the untreated (SUS445, SUS430 and SUS410) and nitrided (SUS445-N) stainless steels in the Ar-saturated 0.5 mol dm^{-3} H_2SO_4 solution at room temperature are presented in Fig. 4-2. Among all the untreated stainless steels, because the SUS445 stainless steel contains the highest content of the corrosion-resisting element, Cr (22.1%), the polarization curve of the SUS445 stainless steel shows an evident passive region and the lowest current densities in both the active and passive regions. For the untreated SUS410 and SUS430 stainless steels, the trend in the polarization curve is similar to that of the SUS445 stainless steel, but the current densities of the SUS410 stainless steel in the active and passive regions are the highest due to the lowest Cr content (11.5~13.0%). Because the stainless steel contains a higher Cr content, a better corrosion resistance is observed. In this study, the nitriding treatment was conducted using the Ni-free SUS445 stainless steel with a good corrosion resistance.

In the case of the nitrided SUS445-N stainless steel, the onset potential shifts toward the positive direction and there is no active current peak compared to the untreated SUS445 stainless steel. Considering the passive behavior, the current densities of the SUS445-N sample are more than one order of magnitude lower than those of the SUS445 sample, indicating a better corrosion resistance than that of the untreated SUS445 stainless steel. Compared to our previous work [25], the nitrided

Ni-free SUS445-N stainless steel prepared in this study was more anti-corrosive and stable. The improved corrosion resistance of the SUS445-N stainless steel can be attributed to the structure and composition change in the surface layer after the nitriding treatment.

The electrochemical result of SUS445-N stainless steel in Fig. 4-2 is slightly different from that of SUS445-N1 stainless steel in Fig. 3-5. The reason can be attributed to the slight difference of nitriding pressures between two stainless steels. It is can be known from the Cr-N phase diagram [28], the nitriding pressure can effect the formation of Cr-N phase.

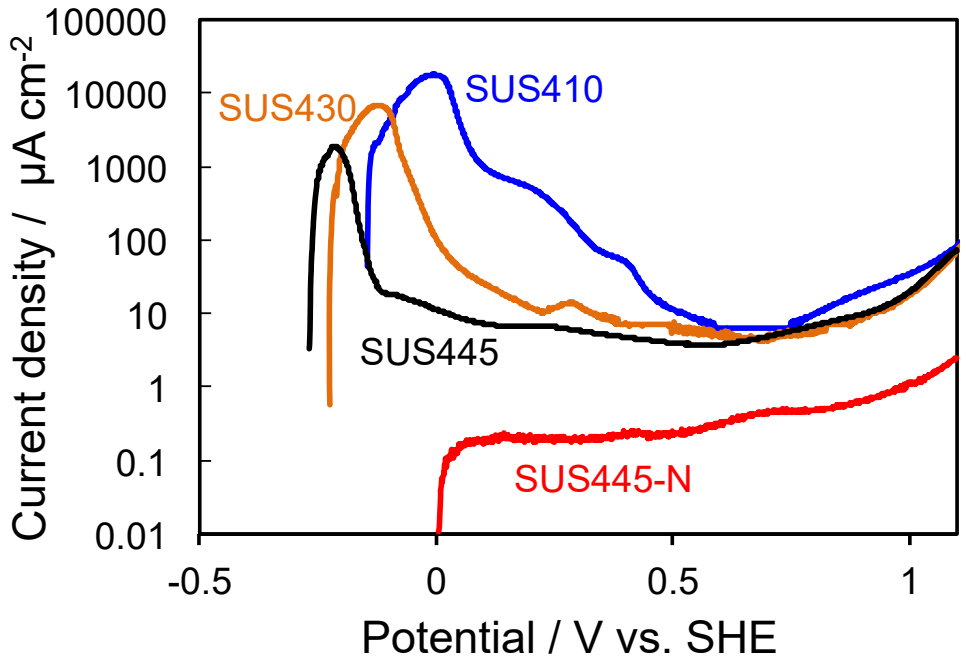

Fig. 4-2. Polarization curves of untreated (SUS445, SUS430 and SUS410) and nitrided (SUS445-N) stainless steels in Ar-saturated 0.5 mol dm^{-3} H_2SO_4 electrolyte at room temperature.

4.3.2 Surface morphology analysis

Figure 4-3 shows SEM images of the untreated SUS445 and nitrided SUS445-N stainless steels before and after the LSV tests. The surface morphology in Fig. 2c was changed compared to the untreated SUS445 stainless steel in Fig. 2a due to the nitriding treatment. After the electrochemical test, the surface of the SUS445 stainless steel was significantly etched, the effect being more visible along the grain boundaries (Fig. 2b). As seen from Fig. 2d, only pitting corrosion occurred on the surface of the nitrided SUS445-N stainless steel after the LSV test. The SEM results suggest that the corrosion resistance of the SUS445-N stainless steel is improved and the corrosion type is pitting corrosion, while the corrosion type of the SUS445 stainless steel is intergranular corrosion.

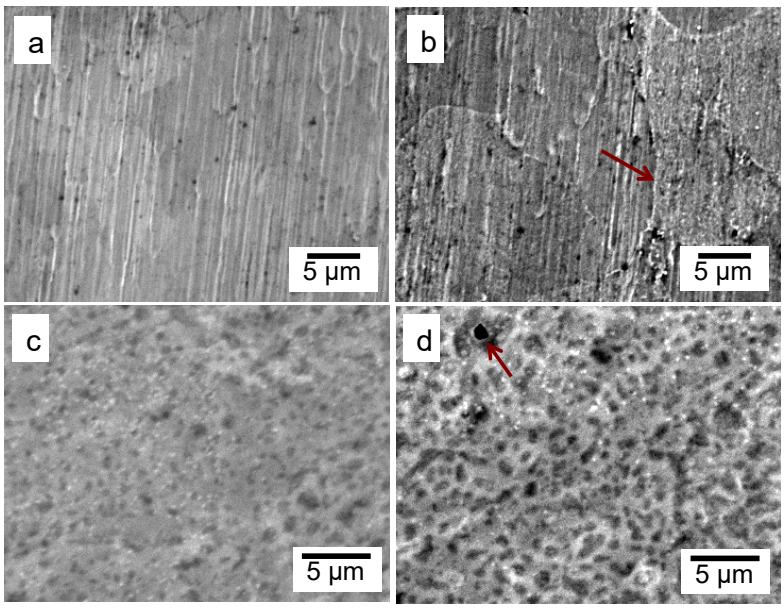

Fig. 4-3. SEM images of untreated SUS445 and nitrided SUS445-N stainless steels before and after LSV measurements.

SUS445 (a) before LSV (b) after LSV; SUS445-N (c) before LSV (d) after LSV.

4.3.3 Surface composition and structure analysis

In order to analyze the surface layer composition of the untreated SUS445 and nitrided SUS445-N stainless steels, the GD-OES profiles were obtained and the results shown in Fig. 4-4. The bare specimen SUS445 has high concentrations of Fe and Cr, while the concentrations of Al, O and N are too low to be detected. The nitrided SUS445-N specimen exhibits a higher concentration of more than 55 at% N after the nitriding treatment, showing that the nitride layer is basically composed of a Cr-N compound.

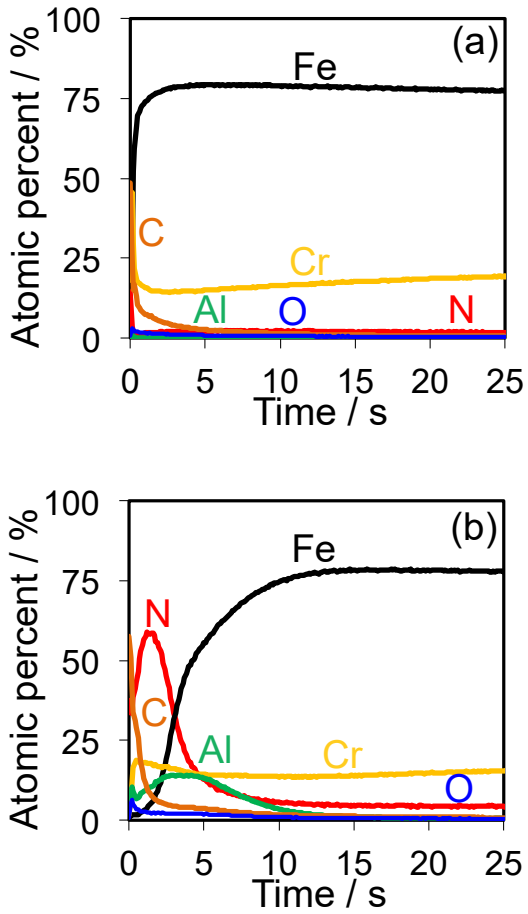

Fig. 4-4. GD-OES results of untreated SUS445 and nitrided SUS445-N stainless steels.

(a) SUS445; (b) SUS445-N.

To more definitively investigate the structure of the outmost regions of the nitride layer, the XRD patterns of the untreated SUS445 and nitrided SUS445-N stainless steels are shown in Fig. 4-5. As for the SUS445, only α-Fe peaks are observed. Compared to the structure of the SUS445 stainless steel, the α-Fe peaks disappeared, while the γ-Fe peaks occurred in the nitride layer of the SUS445-N stainless steel due to the solid solution effect of the nitrogen atoms. In addition to the diffraction peaks of γ-Fe, between 40~80 degree, five additional peaks were detected suggesting that a supersaturated nitrogen phase γ_N [29] and nitrides CrN and Cr_2N were formed after the nitriding treatment. It can be concluded that the nitride layer of the SUS445-N stainless steel consists of γ_N, CrN and Cr_2N phases. At lower angles in Fig. 4, there are other marked peaks that cannot be identified by the comparison with the Standard X-ray Diffraction Powder Patterns.

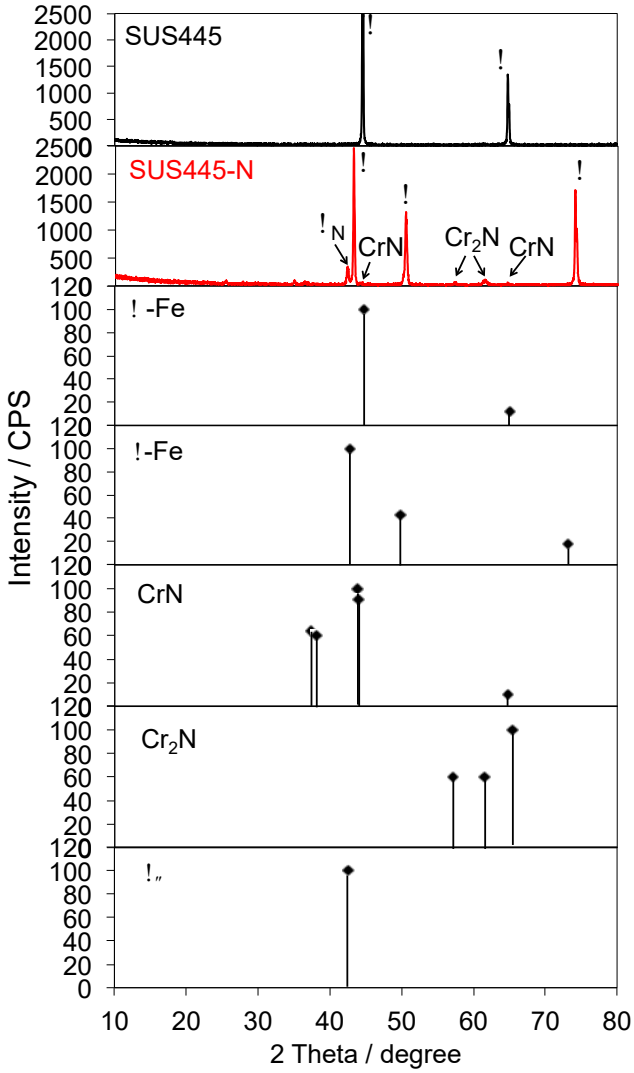

Fig. 4-5. XRD patterns of untreated SUS445 and nitrided SUS445-N stainless steels.

The XPS measurements conducted in this study were used to investigate the chemical states of the N and Cr elements. Fig. 4-6(a) shows the surface XPS N 1s spectra acquired from the nitrided SUS445-N stainless steel taken at different depths. Based on the binding energy value, the peaks at about 397 eV are regarded as nitrides suggesting that the CrN or Cr_2N could be formed [30]. Moreover, the peak at the depth of 75 nm has the strongest intensity. Fig. 4-6(b) shows the XPS Cr 2p profiles of the nitrided SUS445-N stainless steel at the depth of 75 nm. The Cr 2p peaks have

been systematically decomposed into three components as shown in Table 4-3; i.e., a peak at the 574.1 eV corresponding to the metallic Cr, a peak at the 575.6 eV associated with the CrN [31] and a peak at 577.2 eV reflecting the Cr-O bond [32]. The XPS analysis supports the existence of the CrN phase in the nitride layer.

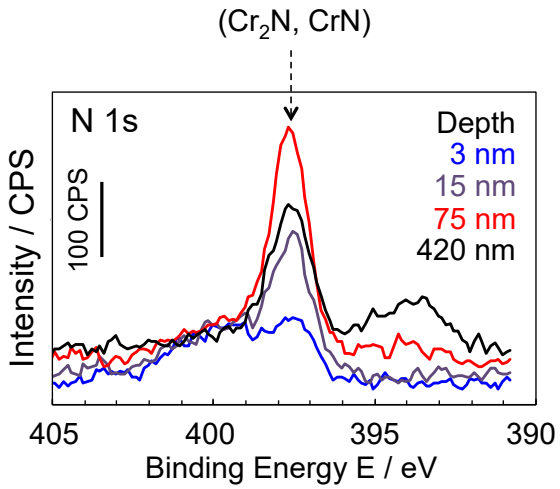

(a) N 1s XPS spectra at different depths

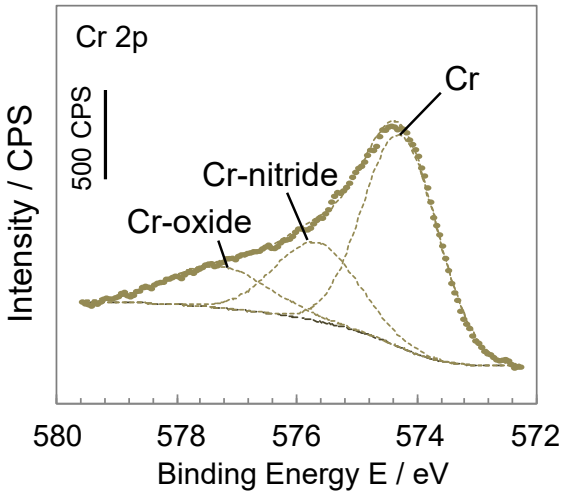

(b) Cr 2p XPS spectra at the depth of 75 nm

Fig. 4-6. XPS spectra of nitrided SUS445-N stainless steel.

(a) N 1s XPS spectra at different depths; (b) Cr 2p XPS spectra at the depth of 75 nm.

Table 4-3. Species in the nitrided SUS445-N stainless steel at the depth of 75 nm.

Species	Chemical bounding	Binding Energy (ev)
Metallic	Cr-Cr	574.1[31]
Defined CrN	Cr-N	575.6[31]
Defined CrO_3 or Cr_2O_3	Cr-O	577.2[32]

The formation of chromium-containing nitrides has been reported in the literature [33, 34]. Brady et al. [33] demonstrated that a dense, continuous and protective CrN/Cr_2N nitride layer was formed on the surface of the Ni-50Cr alloy by thermal gas nitridation, and the corrosion resistance and surface electrical conductivity of the nitrided Ni-50Cr alloy were significantly improved. However, the Ni-base alloys are too far expensive to be used as bipolar plates of PEFCs. Yang et al. [34] reported that it is possible to form a Cr-nitride (CrN and Cr_2N) surface layer by the high-temperature nitridation on V-modified Fe-27Cr base alloys. The Cr-nitride surface layer formed on the model V-modified Fe-27Cr alloys exhibited an excellent corrosion resistance. The XRD and XPS results of this study show that the nitride surface layer composed of the CrN and Cr_2N phases can be formed on the surface of conventional Ni-free SUS445 stainless steels without modification.

4.3.4 Ion plating technology

To confirm the effect of the formed Cr-N phase on the corrosion resistance of the SUS445-N stainless steel, the Cr-N coated SUS445 specimen (Cr-N/SUS445) was prepared by an ion plating technique. The XRD results of the Cr-N/SUS445 stainless steel in Fig. 4-7 prove the formation of the CrN films. The polarization curve of the Cr-N/SUS445 stainless steel was obtained and shown in Fig. 4-8. Also, shown for comparison are data for the untreated SUS445 and nitrided SUS445-N stainless steels. The Cr-N/SUS445 stainless steel was observed to have no active current peak and significantly lower current densities compared to those of the SUS445 stainless steel. The current densities in the passive region of the Cr-N/SUS445 and SUS445-N stainless steels have the same magnitude, but a little higher for the Cr-N/SUS445 stainless steel. Based on the polarization behavior, the CrN and Cr_2N phases formed on the surface of the SUS445-N stainless steel offer an excellent corrosion resistance and the CrN phase is proved very stable according to the LSV measurement prepared by ion plating technique. The supersaturated nitrogen phase γ_N detected by XRD also contributes to the increased corrosion resistance for the SUS445-N stainless steel, resulting in slightly lower current densities than those of the Cr-N/SUS445 stainless steel in the passive region. The effect of the CrN and Cr_2N phases on the improved corrosion resistance of the nitrided SUS445-N stainless steel will be further studied in our future work.

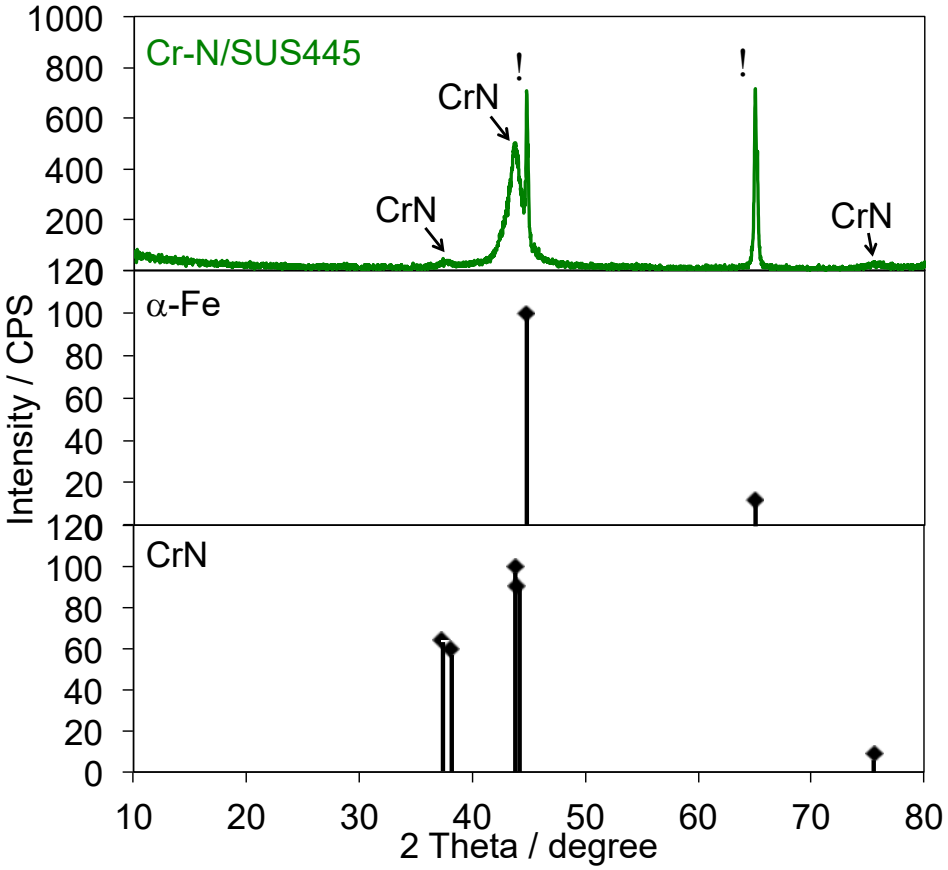

Fig. 4-7. XRD patterns of Cr-N coated SUS445 (Cr-N/SUS445) stainless steel.

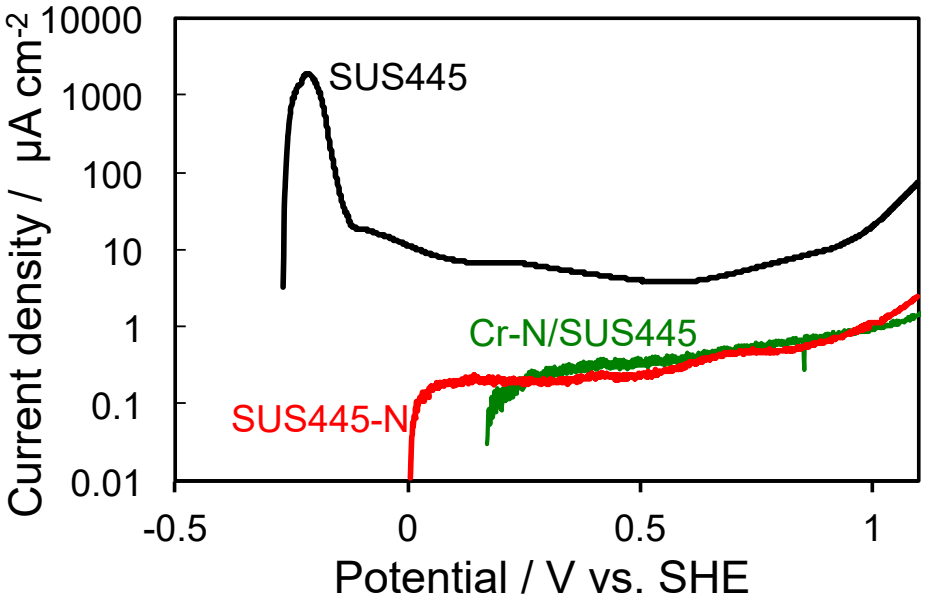

Fig. 4-8. Polarization curves of SUS445, SUS445-N and Cr-N/SUS445 stainless steels in Ar-saturated 0.5 mol dm^{-3} H_2SO_4 electrolyte at room temperature.

4.3.5 Electrical conductivity

The electrical conductivities of the untreated (SUS445, SUS410 and SUS430), nitrided (SUS445-N), Cr-N coated (Cr-N/SUS445) stainless steels and graphite carbon bipolar plate were measured using a Mitsubishi Chemical “Loresta HP” (MCP-T410) electrometer by the four-point probe resistivity technique and the results are listed in Table 4-4. For the SUS445 stainless steel, the resistivity with a 1.5-mm thickness decreases one order of magnitude compared to that with the 0.1-mm thickness suggesting that the thicker the stainless steel, the better the conductivity. The conductivities of the SUS410 stainless steel with a 3.9-mm thickness and graphite carbon bipolar plate with an 18-mm thickness are the best. After the nitriding treatment, the 1.5-mm thick SUS445-N stainless steel showed the same electrical conductivity as that of the untreated 1.5-mm thick SUS445 stainless steel. These results demonstrated that the nitriding treatment improved the corrosion resistance of the Ni-free SUS445 stainless steel without degrading its conductivity.

Table 4-4. Electrical conductivity of each stainless steel and graphite carbon bipolar plate.

Sample name	Thickness / mm	Treatment	Surface resistivity / Ω □$^{-1}$
SUS445	0.1	-	3.17E-02
SUS 445	1.5	-	1.80E-03
SUS 410	3.9	-	2.97E-04
SUS430	1	-	2.32E-03
SUS445-N	1.5	Nitriding	1.63E-03
Cr-N/SUS445	1.5	Ion plating	1.96E-03
Graphite carbon (JARI Cell)	18	-	6.29E-04

4.3.6 Fuel cell durability performance

The Fuel Cell Commercialization Conference of Japan (FCCJ) proposed several methodologies for testing the target performance, durability and cost of fuel cells [35]. We have applied the protocols of the FCCJ to investigate the degradation phenomena and provide an indication of the durability of a JARI standard single cell [36] using the SUS445-N stainless steel as the bipolar plate. Fig. 4-9 shows the fuel cell voltage performance over a period of 2500 h using the SUS445-N and graphite carbon as bipolar plates at 80°C. The current density was 0.25 A cm^{-2}. Based on the test results, the fuel cell voltage performance using the SUS445-N stainless steel as the bipolar plate is almost the same as that using the graphite carbon as the bipolar plate for the 2500 h, and the durability is even slightly better. The results reflect the good corrosion behavior and conductivity of the nitrided SUS445-N stainless steel as the bipolar plate

under conditions similar to the PEFC's operating conditions.

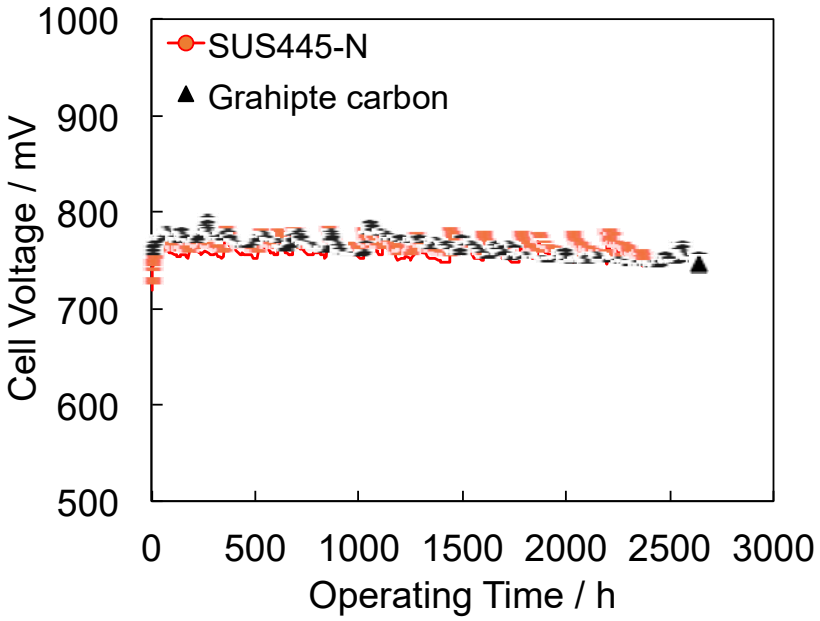

Fig. 4-9. Fuel cell voltage performance over a period of 2500 h using SUS445-N stainless steel and graphite carbon as bipolar plates at 80°C.

4.4 Conclusions

The nitriding treatment of the Ni-free SUS445 stainless steel, which contains a higher content of Cr (22.1%) was conducted at 1200°C in this study. The nitride layer composed of the γ_N, CrN and Cr_2N phases with a good electrical conductivity was formed on the surface of the nitrided SUS445-N stainless steel. The corrosion behaviors of the untreated (SUS445, SUS430 and SUS410) and nitrided (SUS445-N) stainless steels were evaluated in a 0.5 mol dm^{-3} H_2SO_4 solution by the linear sweep voltammetry (LSV) method. The polarization studies indicated that the corrosion resistance of the untreated Ni-free stainless steels is better when containing a higher Cr content. The nitrided SUS445-N stainless steel exhibited a significantly improved corrosion resistance and the corrosion type changed from intergranular corrosion to pitting corrosion.

The electrochemical test of the Cr-N coated SUS445 specimen (Cr-N/SUS445) evaluated the effect of the chromium-containing nitrides formed after the nitriding treatment on the corrosion resistance of the SUS445 stainless steel. The CrN and Cr_2N phases are considered the main reason for the excellent corrosion resistance of the nitrided SUS445-N stainless steel. Our future work will focus on the effect of the CrN and Cr_2N phases on the improved corrosion resistance of the nitrided SUS445-N stainless steel.

The fuel cell durability test was estimated based on the protocols proposed by the Fuel Cell Commercialization Conference of Japan (FCCJ) at 80°C. The fuel cell

voltage performance using the SUS445-N stainless steel as the bipolar plate is almost the same as that using the graphite carbon as the bipolar plate over a period of 2500 h, even slightly better.

References

[1] N. Limjeerajarus, P. Charoen-amornkitt, Effect of different flow field designs and number of channels on performance of a small PEFC, Int. J. Hydrogen Energy, 40 (2015), 7144-7158.

[2] R.F. Silva, D. Franchi, A. Leone, L. Pilloni, A. Masci, A. Pozio, Surface conductivity and stability of metallic bipolar plate materials for polymer electrolyte fuel cells, Electrochim. Acta, 51 (2006), 3592-3598.

[3] A.B. Beleke, K. Miyatake, H. Uchida, M. Watanabe, Gas diffusion electrodes containing sulfonated polyether ionomers for PEFCs, Electrochim. Acta, 53 (2007), 1972-1978.

[4] N. Limjeerajarus, P. Charoen-amornkitt, Effect of different flow field designs and number of channels on performance of a small PEFC, Int. J. Hydrogen Energy, 40 (2015), 7144-7158.

[5] O. M. Orogbemi, D. B. Ingham, M. S. Ismail, K. J. Hughes, L. Ma, M. Pourkashanian, The effects of the composition of microporous layers on the permeability of gas diffusion layers used in polymer electrolyte fuel cells, Int. J. Hydrogen Energy, 41 (2016), 21345-21351.

[6] P. Ekdunge, M. Raberg, The fuel cell vehicle analysis of energy use, emissions and cost, Int. J. Hydrogen Energy, 23 (1998), 381-385.

[7] L.P.L. Carrette, K.A. Friedrich, M. Huber, U. Stimming, Improvement of CO tolerance of proton exchange membrane (PEM) fuel cells by a pulsing technique,

Phys. Chem. Chem. Phys., 3 (2001), 320-324.

[8] C. Coutanceau, R.K. Koffi, J.M. Leger, K. Marestin, R. Mercier, C. Nayoze, P. Capron, Development of materials for mini DMFC working at room temperature for portable applications, J. Power Soures, 160 (2006), 334-339.

[9] W. Zhang, T. Maruta, S. Shironita, M. Umeda, Anode and cathode degradation in a PEFC single cell investigated by electrochemical impedance spectroscopy, Electrochim. Acta, 131 (2014), 245-249.

[10] I. Radev, K. Koutzarov, E. Lefterova, G. Tsotridis, Influence of failure modes on PEFC stack and single cell performance and durability, Int. J. Hydrogen Energy, 38 (2013), 7133-7139.

[11] M. Boaventura, I. Alves, P. Ribeirinha, A. Mendes, The influence of impurities in high temperature polymer electrolyte membrane fuel cells performance, Int. J. Hydrogen Energy, 41 (2016), 19771-19780.

[12] K. Feng, X. Guo, Z. Li, C. Yao, Y. Wu, Investigation of multi-coating process treated magnesium alloy as bipolar plate in polymer electrolyte membrane fuel cell, Int. J. Hydrogen Energy, 41 (2016), 6020-6028.

[13] A. Hermann, T. Chaudhuri, P. Spagnol, Bipolar plates for PEM fuel cells: a review, Int. J. Hydrogen Energy, 30 (2005), 1297-1302.

[14] H. Husby, O. E. Kongstein, A. Oedegaard, F. Seland, Carbon-polymer composite coatings for PEM fuel cell bipolar plates, Int. J. Hydrogen Energy, 39 (2014), 951-957.

[15] Y. Tang, W. Yuan, M. Pan, Z. Wan, Feasibility study of porous copper fiber sintered felt: A novel porous flow field in proton exchange membrane fuel cells, Int. J.

Hydrogen Energy, 35 (2010), 9661-9677.

[16] S. Karimi, N. Fraser, B. Roberts, F.R. Foulkes, A review of metallic bipolar plates for proton exchange membrane fuel cells: materials and fabrication methods, Adv. Mater. Sci. Eng., 2012 (2012), 1-22.

[17] R. Taherian, A review of composite and metallic bipolar plates in proton exchange membrane fuel cell: materials, fabrication, and material selection, J. Power Soures, 265 (2014), 370-390.

[18] Z. Wang, K. Feng, Z. Li, F. Lu, J. Huang, Y. Wu, P. K. Chu, Self-passivating carbon film as bipolar plate protective coating in polymer electrolyte membrane fuel cell, Int. J. Hydrogen Energy, 41 (2016), 5783-5792.

[19] F. Bi, P. Yi, T. Zhou, L. Peng, X. Lai, Effects of Al incorporation on the interfacial conductivity and corrosion resistance of CrN film on SS316L as bipolar plates for proton exchange membrane fuel cells, Int. J. Hydrogen Energy, 40 (2015), 9790-9802.

[20] Y. Show, Electrically conductive amorphous carbon coating on metal bipolar plates for PEFC, Surf Coat Tech, 202 (2007), 1252-1255.

[21] S.J. Lee, C.H. Huang, J.J. Lai, Y.P. Chen, Corrosion-resistant component for PEM fuel cells, J. Power Sources, 131 (2004), 162-168.

[22] H. Tawfik, Y. Hung, D. Mahajan, Metal bipolar plates for PEM fuel cell-a review, J. Power Sources, 163 (2007), 755-767.

[23] K. Lin, X. Li, Y. Sun, X. Luo, H. Dong, Active screen plasma nitriding of 316 stainless steel for the application of bipolar plates in proton exchange membrane fuel cells, Int. J. Hydrogen Energy, 39 (2014), 21470-21479.

[24] K.S. Jung, R.E. Schacherl, E. Bischoff, E.J. Mittemeijer, Nitriding of ferritic Fe-Cr-Al alloys, Surf. Coat. Tech., 204 (2010), 1942-1946.

[25] Y. Yu, S. Shironita, K. Nakatsuyama, K. Souma, M. Umeda, Surface composition effect of nitriding Ni-free stainless steel as bipolar plate of polymer electrolyte fuel cell, Appl. Surf. Sci., 388 (2016), 234-238.

[27] M. Yamashita, M. Agu, Geometrical correction factor for semiconductor resistivity measurements by four-point probe method, Jpn. J. Appl. Phys., 23 (1984), 1499-1504.

[28] Predel, Cr-N (Chromium-Nitrogen), Volume 5d of the series Landolt-Börnstein - Group IV Physical Chemistry, 2012, 1-3.

[29] M.P. Fewell, D.R.G. Mitchell, J.M. Priest, K.T. Short, G.A. Collins, The nature of expanded austenite, Surf. Coat. Technol., 131 (2000), 300-306.

[30] A. Vyas, Y.G. Shen, Z.F. Zhou, K.Y. Li, Nano-structured CrN/CN_x multilayer films deposited by magnetron sputtering, Compos. Sci. Technol., 68 (2008), 2922-2929.

[31] C.D. Wagner, J.F. Moulder, L.E. Davis, and W.M. Riggs, Handbook of X-ray photoelectron spectroscopy, Eden Prairie, USA, 1979.

[32] Y. Ma, L. Wang, Z. Liu, R. Cheng, L. Zhong, Y. Yang, X. He, Y. Fang, M. Terano, B. Liu, High-resolution XPS and DFT investigations into Al-modified Phillips

CrO_x/SiO_2 catalysts, J. Mol. Catal. A Chem, 401 (2015), 1-12.

[33] M.P. Brady, K. Weisbrod, I. Paulauskas, R.A. Buchanan, K.L. More, H. Wang, M. Wilson, F. Garzon, L.R. Walker, Preferential thermal nitridation to form pin-hole free Cr-nitrides to protect proton exchange membrane fuel cell metallic bipolar plates, Scripta Mater., 50 (2004), 1017-1022.

[34] B. Yang, M.P. Brady, H. Wang, J.A. Turner, K.L. More, D.J. Young, P.F. Tortorelli, E.A. Payzant, L.R. Walker, Protective nitride formation on stainless steel alloys for proton exchange membrane fuel cell bipolar plates, J. Power Sources, 174 (2007), 228-236.

[35] A. Iiyama, S. Iguchi, A. Daimaru, K. Shinohara, Objectives, R&D challenge topics and proposed evaluation methods for polymer electrolyte fuel cells, FCCJ (2007).

[36] Y. Hashimasa, T. Numata, K. Moriya, S. Watanabe, Study of fuel cell structure and heating method, Development of JARI's standard single cell, J. Power Sources, 155 (2006), 182-189.

Chapter 5 General conclusions

Nowadays, the potential use of polymer electrolyte fuel cell (PEFC) for residential applications and electric vehicles has been increasingly attracting the attention of researchers. Due to excellent mechanical properties, low volume and good electrical conductivity, stainless steels as alternative materials have been used for bipolar pate in PEFC. However, stainless steels may suffer from corrosion that can degrade the output power of PEFC when contact with the acidic PEFC environment. Now the high cost of PEFC is a big challenge before PEFC application can be commercialized and the bipolar plates account for 21%. In this work, in order to solve the corrosion problem of stainless steel bipolar plate and decrease the cost of PEFC, we investigate the corrosion behavior of Ni-free inexpensive stainless steel used for bipolar plate in PEFC with and without nitriding heat treatment.

Chapter 2 Effect of Cr Content on the Corrosion Resistance of Ni-free Stainless Steels as Bipolar Plate of PEFC

In chapter 2, the corrosion behavior of the four types ferritic stainless steels with different Cr contents have been experimentally investigated to study the effect of Cr content on the corrosion resistance of the ferritic stainless steels as bipolar plate of PEFC in sulfuric acid solution. The results showed that the ferritic stainless steel contains a higher Cr content, a better corrosion resistance is observed.

Chapter 3 Influence of nitriding surface treatment on corrosion characteristics of Ni-free SUS445 stainless steel

In chapter 3, Ni-free SUS445 stainless steels were heat treated under a nitrogen atmosphere at 1473 K and 1373 K, and heat treatment was also performed under an argon atmosphere at 1423 K for comparison. The influence of the nitriding process on the microstructure, morphology, surface element component and corrosion behavior of Ni-free SUS445 stainless steel was investigated. All the nitrided samples showed a better corrosion resistance in the Ar-saturated 0.5 mol dm^{-3} H_2SO_4 solution compared to the untreated and heat-treated samples under an argon atmosphere.

Chapter 4 Corrosion-resistant characteristics of nitrided Ni-free stainless steel for bipolar plate of polymer electrolyte fuel cell

In chapter 4, the nitriding treatment of the Ni-free SUS445 stainless steel, which contains a higher content of Cr (22.1%) was conducted at 1200°C. The nitrided SUS445-N stainless steel exhibited a significantly improved corrosion resistance and the corrosion type changed from intergranular corrosion to pitting corrosion. The nitride layer composed of the γ_N, CrN and Cr_2N phases with a good electrical conductivity was formed on the surface of the nitrided SUS445-N stainless steel. The CrN and Cr_2N phases are considered the main reason for the excellent corrosion resistance of the nitrided SUS445-N stainless steel.

Chapter 5 General conclusions

Nowadays, the potential use of polymer electrolyte fuel cell (PEFC) for residential applications and electric vehicles has been increasingly attracting the attention of researchers. Due to excellent mechanical properties, low volume and good electrical conductivity, stainless steels as alternative materials have been used for bipolar pate in PEFC. However, stainless steels may suffer from corrosion that can degrade the output power of PEFC when contact with the acidic PEFC environment. Now the high cost of PEFC is a big challenge before PEFC application can be commercialized and the bipolar plates account for 21%. In this work, in order to solve the corrosion problem of stainless steel bipolar plate and decrease the cost of PEFC, we investigate the corrosion behavior of Ni-free inexpensive stainless steel used for bipolar plate in PEFC with and without nitriding heat treatment.

Chapter 2 Effect of Cr Content on the Corrosion Resistance of Ni-free Stainless Steels as Bipolar Plate of PEFC

In chapter 2, the corrosion behavior of the four types ferritic stainless steels with different Cr contents have been experimentally investigated to study the effect of Cr content on the corrosion resistance of the ferritic stainless steels as bipolar plate of PEFC in sulfuric acid solution. The results showed that the ferritic stainless steel contains a higher Cr content, a better corrosion resistance is observed.

Chapter 3 Influence of nitriding surface treatment on corrosion characteristics of Ni-free SUS445 stainless steel

In chapter 3, Ni-free SUS445 stainless steels were heat treated under a nitrogen atmosphere at 1473 K and 1373 K, and heat treatment was also performed under an argon atmosphere at 1423 K for comparison. The influence of the nitriding process on the microstructure, morphology, surface element component and corrosion behavior of Ni-free SUS445 stainless steel was investigated. All the nitrided samples showed a better corrosion resistance in the Ar-saturated 0.5 mol dm^{-3} H_2SO_4 solution compared to the untreated and heat-treated samples under an argon atmosphere.

Chapter 4 Corrosion-resistant characteristics of nitrided Ni-free stainless steel for bipolar plate of polymer electrolyte fuel cell

In chapter 4, the nitriding treatment of the Ni-free SUS445 stainless steel, which contains a higher content of Cr (22.1%) was conducted at 1200°C. The nitrided SUS445-N stainless steel exhibited a significantly improved corrosion resistance and the corrosion type changed from intergranular corrosion to pitting corrosion. The nitride layer composed of the γ_N, CrN and Cr_2N phases with a good electrical conductivity was formed on the surface of the nitrided SUS445-N stainless steel. The CrN and Cr_2N phases are considered the main reason for the excellent corrosion resistance of the nitrided SUS445-N stainless steel.

List of publication

(1) **Y. Yu**, S. Shironita, K. Nakatsuyama, K. Souma, M. Umeda, Surface composition effect of nitriding Ni-free stainless steel as bipolar plate of polymer electrolyte fuel cell, Appl. Surf. Sci., 388 (2016), 234-238.

(2) **Y. Yu**, S. Shironita, K. Nakatsuyama, K. Souma and M. Umeda, Influence of Nitriding Surface Treatment on Corrosion Characteristics of Ni-free SUS445 Stainless Steel, Electrochemistry, 84 (9) (2016), 709-713.

(3) **Y. Yu**, S. Shironita, T. Mizukami, K. Nakatsuyama, K. Souma, M. Umeda, Corrosion-resistant characteristics of nitrided Ni-free stainless steel for bipolar plate of polymer electrolyte fuel cell, Int. J. Hydrogen Energy, 42 (2017), 6303-6309.

Reference publication

(1) **Yu Yang**, Neil Ihsan, 白仁田 沙代子, 中津山 國雄, 相馬 憲一, 梅田 実, 固体高分子形燃料電池用金属セパレータとしての Ni フリーステンレス鋼における表面化学組成の影響, 燃料電池, 16(3) (2017), 67-72.